1

Direct numerical simulation of $H_2/O_2/N_2$ flames with complex chemistry in two-dimensional turbulent flows

By M. BAUM[1], T. J. POINSOT[2], D. C. HAWORTH[3]
AND N. DARABIHA[1]

[1] Laboratoire EM2C, CNRS, Ecole Centrale, Paris

[2] Centre de Recherche sur la Combustion Turbulente and IMFT/CERFACS, 42 av. G. Coriolis, 31057 Toulouse, France

[3] General Motors NAO Research and Development Center, Warren, MI 48090, USA

Premixed $H_2/O_2/N_2$ flames propagating in two-dimensional turbulence have been studied using direct numerical simulations (DNS: simulations in which all fluid and thermochemical scales are fully resolved). Simulations include realistic chemical kinetics and molecular transport over a range of equivalence ratios Φ ($\Phi = 0.35, 0.5, 0.7, 1.0, 1.3$). The validity of the flamelet assumption for premixed turbulent flames is checked by comparing DNS data and results obtained for steady strained premixed flames with the same chemistry (flamelet 'library'). This comparison shows that flamelet libraries overestimate the influence of stretch on flame structure. Results are also compared with earlier zero-chemistry (flame sheet) and one-step chemistry simulations. Consistent with the simpler models, the turbulent flame with realistic chemistry aligns preferentially with extensive strain rates in the tangent plane and flame curvature probability density functions are close to symmetric with near-zero means. For very lean flames it is also found that the local flame structure correlates with curvature as predicted by DNS based on simple chemistry. However, for richer flames, by contrast to simple-chemistry results with non-unity Lewis numbers (ratio of thermal to species diffusivity), local flame structure does not correlate with curvature but rather with tangential strain rate. Turbulent straining results in substantial thinning of the flame relative to the steady unstrained laminar case. Heat-release and H_2O_2 contours remain thin and connected ('flamelet-like') while species including H-atom and OH are more diffuse. Peak OH concentration occurs well behind the peak heat-release zone when the flame temperature is high (of the order of 2800 K). For cooler and leaner flames (about 1600 K and for an equivalence ratio below 0.5) the OH radical is concentrated near the reaction zone and the maximum OH level provides an estimate of the local flamelet speed as assumed by Becker *et al.* (1990).

1. Introduction

Turbulent premixed combustion in practical devices is a complex phenomenon combining chemical kinetics, molecular transport, and hydrodynamic turbulence in difficult geometric configurations. Increasing regulative and competitive pressures demand improved physical understanding and predictive modelling capability for combustion phenomena including ignition, quenching, and pollutant formation. For example, many governments impose limits on emissions of oxides of nitrogen, carbon

monoxide, and unburned hydrocarbons from gasoline-fuelled spark-ignited automotive engines. Pending regulations in the United States seek further reductions in the allowable levels of these pollutants and provide for species differentiation in hydrocarbon emissions to account for the relative propensity of different components to promote ozone formation in the atmosphere. Many aspects of chemical kinetics (e.g. aromatic hydrocarbon chemistry, Westbrook & Dryer 1984) are poorly understood even at a fundamental level and emissions models for engineering applications remain largely empirical. Thus complex chemical kinetics in turbulent premixed combustion is a crucial topic for research and modelling.

Both experimental and numerical investigations of chemical kinetics influences in turbulent premixed combustion are complicated by the strong coupling of hydrodynamics with thermochemistry and by resolution requirements: hydrodynamic and thermochemical spatial and temporal scales span many orders of magnitude in premixed flames at high Reynolds and Damköhler numbers (the latter being the ratio of a characteristic flow timescale to chemical timescales). Thus direct numerical simulation (DNS) of practical turbulent premixed flames is impracticable at present and will remain so for the foreseeable future. Here and in the following 'DNS' is taken to mean simulations in which all scales of motion are fully resolved both spatially and temporally so that no turbulence modelling – explicit spatial or temporal filtering – is employed.

Numerical combustion studies have tended to proceed along one of two parallel paths. Either detailed chemical kinetics models have been implemented in simple flow configurations (one-dimensional laminar, e.g. Warnatz 1981; Drake & Blint 1988; Axisymmetric laminar, e.g. Smooke *et al.* 1990, or turbulence simulations have been performed with embedded simple-chemistry models (zero-chemistry or flame sheet, e.g. Kerstein, Ashurst & Williams 1988; Girimaji & Pope 1992; zero-heat-release one-step Arrhenius, e.g. Rutland, Ferziger & El Tahry 1990; one-step Arrhenius with heat release, e.g. Haworth & Poinsot 1992). The detailed chemistry scheme for methane–air oxidation employed by Xu & Smooke (1991) includes 26 species and 45 reactions. Solving the resulting stiff system of convection/diffusion/reaction equations for a *laminar* axisymmetric Bunsen-burner flame requires on the order of 100 CPU hours using state-of-the-art numerical algorithms on a high-end workstation ($\sim$ 26 Mflops). This is the same order of computational resources as that required for DNS of *nonreacting* homogeneous isotropic turbulence at a Taylor-scale Reynolds number of $Re_\lambda \approx 90$ (Pope 1991).

The present research represents an attempt to bridge the two numerical approaches by coupling complex chemistry and full turbulence simulations. Here H_2–O_2 chemistry (inert N_2 diluent) has been modelled using a nine-species, 19-reactant scheme (Miller *et al.* 1982) including detailed molecular transport in two-dimensional isotropic turbulence. Specific goals are threefold.

First, we wish to explore the feasibility of complex-chemistry DNS for future application to more complex thermochemical systems (e.g. hydrocarbon fuels). Ignition, quenching, and pollutant formation issues are of practical interest in such systems.

Secondly, we will compare results obtained using the present detailed-chemistry scheme to those obtained earlier using simpler zero- and one-step chemistry models. In particular we are interested in statistics of strain rate, curvature, and local burning rate along the flame front. We will also consider the profile of the OH radical to determine when OH is a good tracer of the reaction zone as assumed in many experimental studies.

Finally, we will compare the local structure of the turbulent premixed flame with detailed kinetics to that of steady strained and unstrained laminar flames having the same thermochemical properties to check the robustness of flamelet models with realistic kinetics.

2. Background: DNS of turbulent premixed combustion

DNS has proved to be a valuable tool in addressing fundamental physical questions and in the construction of models for turbulent premixed combustion. The past several years have seen DNS applied to a hierarchy of premixed systems of increasing complexity. Results of these simulations generally have been interpreted in the framework of the flamelet regime of combustion where a thin laminar-like reaction zone separates unburnt gas from hot burnt products. (In propagating-interface type models, this structure is imposed.) Roughly speaking, flamelet combustion corresponds to conditions where the largest chemical scales are small compared with the smallest hydrodynamic scales: however, it has proved to be a worthwhile framework in which to interpret results even in cases where turbulence microscales are smaller than the flame thickness (Haworth & Poinsot 1992). Moreover, flamelet models are widely used as combustion 'submodels' in Reynolds-averaged computations of premixed turbulent combustion in engineering applications (El Tahry 1990; Boudier *et al.* 1992).

2.1. *Propagating-interface (zero-chemistry) models*

Analytic studies of the kinematics of a propagating surface in turbulent flow have resulted in relationships that provide a basis for flamelet models and for interpreting numerical simulation results. For example, the role of hydrodynamic straining and flame curvature in modifying the area A of a propagating surface element are expressed in the relationship (Pope 1988; Candel & Poinsot 1990),

$$\frac{1}{A}\frac{dA}{dt} = a_t + \frac{s_d}{\mathscr{R}}. \tag{1}$$

Here a_t is the hydrodynamic strain rate in the plane tangent to the surface, s_d is the speed of advance of the propagating surface relative to the fresh gas, and $\mathscr{R}$ is the radius of curvature ($\mathscr{R} < 0$ for surface elements propagating towards the centre of curvature, e.g. concave towards reactants for the premixed flame). This relationship motivates attempts to isolate strain-rate from curvature effects in turbulent premixed combustion, even though the two are not completely independent (Pope 1988; Haworth & Poinsot 1992).

Numerical simulations (DNS) incorporating propagating surface models have proceeded via a variety of front-tracking algorithms (reviewed in Oran & Boris 1987, pp. 416–431), field-equation approaches (Kerstein *et al.* 1988; Ashurst, Sivashinsky & Yakhot 1988), and statistical ensembles of infinitesimal surface elements (Girimaji & Pope 1992). These zero-chemistry flame-sheet models have contributed significantly to our understanding of flame topology and have provided quantitative information on statistical correlations that is useful in the construction and calibration of models of turbulent premixed combustion in the flamelet regime (Bray & Cant, 1991). The influence of chemical kinetics effects in such models generally is felt only through the propagation speed, whose dependence on thermochemical and/or turbulence parameters must be prescribed.

2.2. *Simple-chemistry models*

Studies of the dynamic interactions between fluid flow and finite-rate chemistry in flamelet or non-flamelet regimes require that the flame structure be resolved. However, the addition of chemical length- and timescales that are of the order of or smaller than the smallest turbulence scales implies that, for a given spatial and temporal resolution, a smaller range of hydrodynamic scales can be simulated compared to computations in which the flame has no internal structure. Two-dimensional vortex methods have been used to study interactions between turbulent fluid flow and finite-rate chemistry by a number of authors including Ashurst & Barr (1983), Ghoniem & Krishnan (1988), and Ashurst, Peters & Smooke (1987). Three-dimensional simulations including finite-rate chemistry (constant density, zero heat release, single-step Arrhenius chemistry) have been reported by Rutland *et al.* (1990): results included distributions of local burning rate over a range of Damköhler numbers. Further three-dimensional constant-density simulations have been published by El Tahry, Rutland & Ferziger (1991), Rutland & Trouvé (1990) (a study of Lewis number effects), Rutland & Trouvé (1993) and by Cant, Rutland & Trouvé (1990) (a study of statistics relevant to the Bray–Moss–Libby model of turbulent premixed combustion). A one-step reduced mechanism has been implemented recently in a DNS study of non-premixed turbulent combustion (three-dimensional, constant property) by Montgomery, Kosaly & Riley (1993).

The present work follows a number of two-dimensional simulations with variable fluid properties and heat release (Poinsot 1991; Poinsot, Veynante & Candel 1990, 1991; Poinsot, Echekki & Mungal 1992; Poinsot, Haworth & Bruneaux 1993; Meneveau & Poinsot 1990; Haworth & Poinsot 1992). Contributions of these studies include a characterization of the scales of turbulent motion that influence flame structure (Poinsot *et al.* 1990; Poinsot 1991), investigations of flame quenching (Poinsot *et al.* 1991; Meneveau & Poinsot 1990), identification of Lewis number effects (Haworth & Poinsot 1992), a study of ignition and early flame-kernel growth (Poinsot 1991), and a model for flame–wall interactions (Poinsot *et al.* 1993). After these initial studies, two approaches have been followed: three-dimensional DNS with heat release but simple chemistry (Trouvé & Poinsot 1994) and in the present paper two-dimensional DNS with complex chemistry. Compared to three-dimensional cases, two-dimensional DNS allows larger turbulent Reynolds numbers (up to 1000) and a wider dynamic range of lengthscales. Values of relevant dimensionless parameters in the present study are given in §3.

However, the dynamics of two-dimensional turbulence are not identical to those of three-dimensional turbulence (Batchelor 1953; Herring *et al.* 1974; Lesieur 1987). In particular, the vortex-stretching mechanism for the cascade of energy to progressively smaller scales of motion is absent in two dimensions and the smallest scales of motion do not follow the usual Kolmogorov scaling. Thus the statistics of small-scale quantities especially are expected to differ between two-dimensional and three-dimensional simulations. Partial justification for the appropriateness of two-dimensional studies of premixed flame structure can be found in three-dimensional results: the topology of a propagating surface in three-dimensional turbulence has been found to be primarily two-dimensional, particularly those surface elements having the highest curvatures (Ashurst 1990; Cant *et al.* 1990; Girimaji & Pope 1992). That is, a flame tends to be locally cylindrical rather than spherical in shape. Further *a posteriori* justification can be found in the two-dimensional results themselves, where many features in common with the three-dimensional findings have been noted (Haworth & Poinsot 1992; Trouvé & Poinsot 1994). Common results include: preferential alignment

of the flame with extensive strain rates in the tangent plane; scaling of flame-area-averaged mean tangential strain rate with turbulence micro-timescales; and close to symmetric p.d.f.'s of flame curvature having near-zero mean.

The present work follows most immediately the study of non-unity Lewis number effects (Le = ratio of thermal to species diffusivity) in two-dimensional turbulent premixed combustion reported by Haworth & Poinsot (1992). In addition to the results already discussed, it was found that for $Le = 1$, local burning velocity of the turbulent flame is everywhere nearly identical to that of a steady unstrained laminar flame; for non-unity Lewis numbers, the local burning velocity differs from that of the laminar flame and correlates strongly with the local flame curvature; curvature effects cancel out in the mean to leave the mean extensive tangential strain rate as the principal influence on the mean burning velocity of the turbulent flame; and thermodiffusive effects result in more flame area for $Le < 1$ than for $Le > 1$. It was further argued that these molecular transport effects should remain important at higher Reynolds number and for complex chemistry, provided that a single global deficient-reactant-based Lewis number can be defined. Here the simulations are extended from one-step chemistry with simple transport to realistic chemistry and transport, permitting a direct assessment of the second claim. We continue to adopt a flamelet viewpoint for diagnostics and analysis.

3. Problem definition

3.1 *Governing equations and numerical methods*

The set of equations solved is the compressible multi-species reacting flow equations comprising conservation of mass, linear momentum, energy, and N_s species mass fractions. In Cartesian tensor notation (no sum on Greek indices)

$$\frac{\partial \rho}{\partial t} + \frac{\partial \rho u_j}{\partial x_j} = 0, \tag{2}$$

$$\frac{\partial \rho u_i}{\partial t} + \frac{\partial \rho u_i u_j}{\partial x_j} = -\frac{\partial p}{\partial x_i} + \frac{\partial \tau_{ij}}{\partial x_i}, \tag{3}$$

$$\frac{\partial \rho e_t}{\partial t} + \frac{\partial (\rho e_t + p) u_j}{\partial x_j} = \frac{\partial (u_j \tau_{ij})}{\partial x_i} - \frac{\partial q_j}{\partial x_j}, \tag{4}$$

$$\frac{\partial \rho Y_\alpha}{\partial t} + \frac{\partial \rho Y_\alpha u_j}{\partial x_j} = -\frac{\partial \rho Y_\alpha V_{\alpha j}}{\partial x_j} + W_\alpha \dot{\omega}_\alpha. \tag{5}$$

Here u_i is the ith component of the fluid velocity, e_t is the total energy density per unit mass, and Y_α, $\alpha = 1, ..., N_s$, is the mass fraction of species α. The fluid mass density is ρ, p is the thermodynamic pressure, and τ_{ij} and q_j are, respectively, the viscous stress tensor and the heat flux vector. The molar chemical production rate of species α is $\dot{\omega}_\alpha$ while W_α is its molecular weight. The variable $V_{\alpha j}$ is the diffusion velocity for species α.

The set of governing equations is closed with the ideal-gas equation of state and constitutive relations,

$$p = \rho RT, \tag{6}$$

$$\tau_{ij} = \bar{\mu} \left(\frac{\partial u_i}{\partial x_j} + \frac{\partial u_j}{\partial x_i} - \frac{2}{3} \delta_{ij} \sum_{k=1}^{3} \frac{\partial u_k}{\partial x_k} \right), \tag{7}$$

$$e_t = \frac{1}{2} \sum_{k=1}^{3} u_k u_k + e, \tag{8}$$

$$e = \sum_{\alpha=1}^{N_s} h_\alpha Y_\alpha - \frac{p}{\rho}, \tag{9}$$

$$h_\alpha(T_1) = \Delta h_{f\alpha}^0 + \int_{T_0}^{T_1} C_{p\alpha}(T)\,\mathrm{d}T, \tag{10}$$

$$q_j = -\bar{\lambda}\frac{\partial T}{\partial x_j} + \rho \sum_{\alpha=1}^{N_s} h_\alpha Y_\alpha V_{\alpha j}. \tag{11}$$

In these equations, $\bar{\mu}$ and $\bar{\lambda}$ are, respectively, the mixture mean viscosity and thermal conductivity. The formation enthalpy of species α at the reference temperature T_0 is $\Delta h_{f\alpha}^0$, and h_α is the enthalpy of species α. (Here the reference state is $T_0 = 298.15\ K$.)

Species molecular transport is modelled using Fick's law. The diffusion coefficient D_α of the species α in the mixture is computed as follows:

$$D_\alpha = \frac{1 - Y_\alpha}{\sum_{\beta=1, \beta \neq \alpha}^{N_s} X_\beta/D_{\alpha\beta}}, \tag{12}$$

where $D_{\alpha\beta}$ are the binary diffusion coefficients and X_α is the mole fraction of species α. Diffusion coefficients are related to the diffusion velocity $\mathcal{V}_{\alpha j}$ by

$$\mathcal{V}_{\alpha j} = -\frac{D_\alpha}{X_\alpha}\frac{\partial X_\alpha}{\partial x_j}. \tag{13}$$

The diffusion velocities resulting from (12) and (13) does not, in general, satisfy conservation of mass. A correction velocity V_{cj} is added such that the net diffusive flux is equal to zero:

$$\sum_{\alpha=1}^{N_s} Y_\alpha V_{\alpha j} = 0, \tag{14}$$

with $$V_{\alpha j} = \mathcal{V}_{\alpha j} + V_{cj} = -\frac{D_\alpha}{X_\alpha}\frac{\partial X_\alpha}{\partial x_j} + \sum_{\beta=1}^{N_s} Y_\beta(D_\beta/X_\beta)\frac{\partial X_\beta}{\partial x_j}. \tag{15}$$

Species production rates are given by the Arrhenius law with (forward) rate constants k_{fr} of the form

$$k_{fr} = A_r T^{b_r} \exp(-E_{0r}/R_0 T), \tag{16}$$

where R_0 is the universal gas constant. Detailed reaction mechanisms for hydrogen–oxygen kinetics may be found in many studies (Miller *et al.* 1982; Kee *et al.* 1988; Dixon-Lewis & Missaghi 1988). Darabiha & Candel (1992) show that all these schemes provide similar results in the laminar counterflow diffusion flame configuration proposed by Dixon-Lewis & Missaghi (1988). Ambient conditions (atmospheric pressure and a temperature of 300 K) were used while the mole fraction of hydrogen ranged from $X_{H_2} = 0.21$ to $X_{H_2} = 0.5$. Similarity of results was checked by comparing Arrhenius plots (reaction rate versus inverse of temperature where temperature ranges from 300 to 2800 K), the extinction limits, and the flame response to strain (from 0 to the extinction limits). Thus for computational convenience we chose the nine-species, 19-reaction scheme devised by Miller *et al.* (1982) in the present study. Coefficients for this scheme are summarized in table 1. Fluid properties, molecular transport

No.	Reaction	A	b	E_0
R_1	$H_2+O_2 \rightleftharpoons 2OH$	1.7×10^{13}	0	47780
R_2	$H_2+OH \rightleftharpoons H_2O+H$	1.17×10^9	1.3	3626
R_3	$H+O_2 \rightleftharpoons OH+O$	5.13×10^{16}	-0.816	16507
R_4	$O+H_2 \rightleftharpoons OH+H$	1.8×10^{10}	1.0	8826
R_5	$H+O_2+M \rightleftharpoons HO_2+M^a$	2.1×10^{18}	-1.0	0
R_6	$H+2O_2 \rightleftharpoons HO_2+O_2$	6.7×10^{19}	-1.42	0
R_7	$H+O_2+N_2 \rightleftharpoons HO_2+N_2$	6.7×10^{19}	-1.42	0
R_8	$OH+HO_2 \rightleftharpoons H_2O+O_2$	5×10^{13}	0	1000
R_9	$H+HO_2 \rightleftharpoons 2OH$	2.5×10^{14}	0	1900
R_{10}	$O+HO_2 \rightleftharpoons O_2+OH$	4.8×10^{13}	0	1000
R_{11}	$2OH \rightleftharpoons O+H_2O$	6×10^8	1.3	0
R_{12}	$H_2+M \rightleftharpoons H+H+M^b$	2.23×10^{12}	0.5	92600
R_{13}	$O_2+M \rightleftharpoons O+O+M$	1.85×10^{11}	0.5	95560
R_{14}	$H+OH+M \rightleftharpoons H_2O+M^c$	7.5×10^{23}	-2.6	0
R_{15}	$HO_2+H \rightleftharpoons H_2+O_2$	2.5×10^{13}	0	700
R_{16}	$2HO_2 \rightleftharpoons H_2O_2+O_2$	2×10^{12}	0	0
R_{17}	$H_2O_2+M \rightleftharpoons OH+OH+M$	1.3×10^{17}	0	45500
R_{18}	$H_2O_2+H \rightleftharpoons H_2+HO_2$	1.6×10^{12}	0	3800
R_{19}	$H_2O_2+OH \rightleftharpoons H_2O+HO_2$	1.0×10^{13}	0	1800

[a] Third-body efficiencies: $k(H_2) = 3.3k(Ar)$ $k(H_2O) = 21.0(Ar)$.
[b] Third-body efficiencies: $k(H_2) = 3.0k(Ar)$ $k(H) = 2.0k(Ar)$ $k(H_2O) = 6.0k(Ar)$.
[c] Third-body efficiencies: $k(H_2O) = 20.0k(Ar)$.

TABLE 1. Reaction mechanism by Miller *et al.* (1982). Reaction mechanism rate coefficients are in the form $k_f = AT^b \exp(-E_0/R_0 T)$ (Miller *et al.* 1982) in s-cm³-cal-mol-K units. Species: H_2, O_2, OH, O, H, H_2O, HO_2, H_2O_2, N_2.

coefficients, and production terms are computed using CHEMKIN and TRANSPORT packages (Kee, Miller & Jefferson 1980; Kee, Warnatz & Miller 1983) in their vectorized form (Darabiha *et al.* 1989).

Despite the fact that thermal diffusion was not included in the present approach (Dixon-Lewis & Williams 1979), the computed velocities agree well with published results (Warnatz 1981) within uncertainty limits. The neglect of thermal diffusion of the species leads to an increase of 5% to 6% in the burning velocity (essentially due to the H-radical).

Using these assumptions and a Cartesian frame of reference, the conservation equations are solved using a high-order finite-difference scheme (Lele 1992). The calculations are initialized with reactants on one side of the computational domain and products on the other; these are separated by a flat laminar premixed flame (figure 1). The initial laminar profiles are themselves steady one-dimensional solutions to (2)–(16). On lateral boundaries, periodic conditions are enforced while non-reflecting boundary conditions are used on inflow/outflow boundaries (Poinsot & Lele 1992). Isotropic two-dimensional turbulence is prescribed with a turbulence energy spectrum $E(k)$ of von Kármán enhanced by Pao (Hinze 1975),

$$E(K) = A \frac{u'^5(K_e, K_d)}{\epsilon(K_e, K_d)} \frac{(K/K_e)^4}{[1+(K/K_e)^2]^{17/6}} \exp\left[-\tfrac{3}{2}\alpha \left(\frac{K}{K_d}\right)^{4/3} \right], \qquad (17)$$

with coefficients $A = 1.5$ and $\alpha = 1.5$, K_e the wavenumber of the most energetic vortices, and K_d the wavenumber of the Kolmogorov scale. The implementation is the same as that used in earlier studies (Haworth & Poinsot 1992). Two parameters define the initial energy spectrum: the peak-energy wavelength $L_i = 2\pi/K_e$ and the
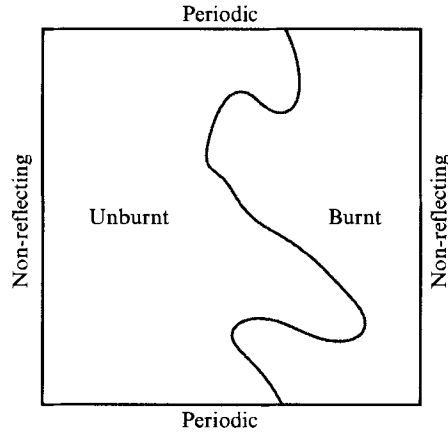
FIGURE 1. Schematic of computational domain: a premixed flame separates unburnt reactants from burnt products.

Case	Φ	$X_{O_2}/(X_{O_2}+X_{N_2})$	X_{H_2}	X_{O_2}	X_{N_2}	T_u (K)	p (kPa)	s_l^0 (m s^{-1})	δ_l (cm)
1, 2, 3	1.0	0.330	0.400	0.200	0.400	800	101	19.5	0.042
4, 5	0.7	0.277	0.280	0.200	0.520	800	101	14.6	0.045
6	0.5	0.250	0.200	0.200	0.600	800	101	10.8	0.048
7, 8	1.3	0.417	0.520	0.200	0.280	800	101	23.8	0.037
9	0.5	0.21	0.173	0.173	0.654	300	101	0.67	0.393
10	0.35	0.21	0.128	0.183	0.689	300	101	0.11	0.100

TABLE 2. Initial chemical parameters

Kolmogorov wavelength $L_d = 2\pi/K_d$ which fix the initial r.m.s. turbulence velocity u' and the initial turbulence dissipation rate ϵ so that $k = 3/2u'^2$ satisfies the relation

$$k = \int_0^\infty E(K)\,dK, \tag{18}$$

and

$$\epsilon = \int_0^\infty 2\nu K^2 E(K)\,dK. \tag{19}$$

These and other relevant parameters are summarized in tables 2 and 3.

In tables 2 and 3, a subscript u refers to properties in the unburnt reactants. Key parameters are: the r.m.s. turbulence intensity u', the turbulence integral lengthscale l based on two-point velocity correlations and timescale $\tau = l/u'$, and flame or chemical scales s_l^0 (the unstrained laminar flame speed), $\delta_l \equiv (T_b - T_u)/(dT/dx|_{max})$ (the laminar flame thickness), and $\tau_f = \delta_l/s_l^0$. The fuel mass equivalence ratio is Φ. There are $n_x \times n_y$ computational grid points in the $L_{box} \times L_{box}$ square computational domain. The different values for the molar fractions X_{H_2}, X_{O_2}, X_{N_2} (table 2) or the temperature T_u correspond to practical limits imposed by computer resources. For example the code efficiency increases when the flame speed increases: this explains why oxygen-enriched mixtures have been used for cases 1–8.

The turbulence Reynolds numbers and ratio of r.m.s. turbulence intensity to laminar flame speed of table 3 imply a regime of combustion where turbulence is intense compared to the laminar flame speed, and flames are thinner than the turbulence
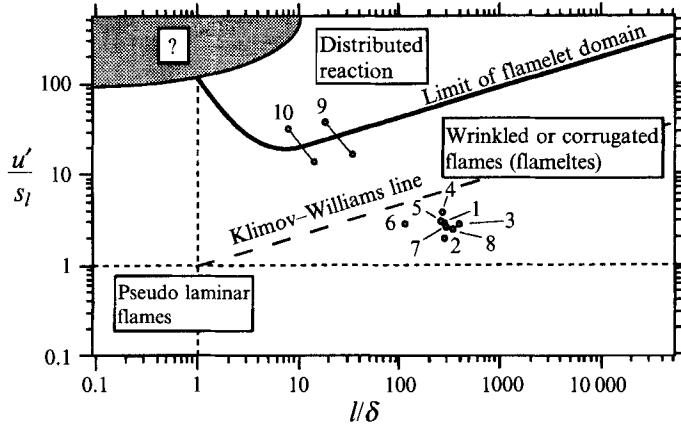
FIGURE 2. Premixed turbulent combustion diagram (Poinsot *et al.* 1993).

Case	$Re_{Lt} = u'L_t/\nu$	$Re_t = u'l/\nu$	u'/s_l^0	L_t/δ_t	l/δ_t	τ/τ_f	L_{box}	$n_x = n_y$
1	5964	607	2.68	29.3	2.91	1.09	1.24	301
2	2647	278	1.23	29.3	2.88	2.34	1.24	301
3	11056	959	2.68	50.0	4.34	1.62	2.00	487
4	5985	600	3.15	27.5	2.71	0.86	1.24	301
5	5326	531	2.68	28.2	2.81	1.04	1.24	301
6	2880	275	2.67	28.1	2.78	1.04	1.24	301
7	4800	598	2.68	23.0	2.87	1.07	1.41	601
8	7172	926	2.67	33.3	4.34	1.62	1.41	601
9	4809	613	30.6	9.89	1.26	0.041	0.90	601
10	2227	289	30.9	10.7	1.39	0.045	2.50	601

TABLE 3. Initial turbulence parameters

integral scale but are thicker than turbulence microscales. Initial turbulence and flame timescales are of the same order for cases 1–8. Corresponding points are indicated in the usual turbulent combustion diagram of figure 2. For cases 9 and 10 initial as well as final conditions are given. In this diagram, the flame lengthscale used to non-dimensionalize the integral lengthscale l is not the laminar flame thickness δ_l, but a flame thickness δ defined by $\delta s_l^0/\nu = 1$ to follow definitions of other authors. Except for the initial values of cases 9 and 10 these simulations appear to be below recent limits (Poinsot *et al.* 1991), which have been shown to be representative of the flamelet regime. Indeed, results will show that, to first order, all flames retain a 'flamelet-like' structure.

Present turbulence Reynolds numbers and the normalized turbulence intensity u'/s_l^0 (table 3) are typical of values found, for example, in reciprocating internal combustion (IC) engines at low engine speeds. The computed flames remain thick compared to the $l/\delta_l \approx 30$ typical of propane–air mixtures under standard IC-engine operating conditions (stoichiometric, $p = 5$ atm, $T_u = 600$ K, undiluted). However, l/δ_l can be as low as three for high T_u, low p, or high exhaust-gas dilution engine cases (Mantzaras, Felton & Bracco 1988; Blint 1988, 1991).

For these cases, turbulence decay is reasonably small and leads to turbulent kinetic energy changes of 60% for cases 9 and 10 and only 8% for the other cases between the initial time and the end of simulation. The box is chosen so that (within simulation time) the flame does not escape from the domain. In typical cases it propagates 6

laminar flame thicknesses or about 2 integral lengthscales. Typical computation times are 100 CPU hours on a CRAY-C98 (mono-processor; the same cases with simple chemistry and transport models would require 10 CPU hours).

3.2. *Diagnostics*

Postprocessing of the two-dimensional computed fields (snapshots at fixed times) begins by defining a flame front as an isocontour of reactant mass fraction or temperature. Here we have used $Y_{O_2} = 0.22$, corresponding to the position of peak heat release in the laminar flame for $\Phi = 1.0$ (figure 4). Once the flame front has been located, the local normal and local curvature are readily computed. Curvatures concave towards the hot products are taken to be positive. One-dimensional cuts normal to the flame are taken to define the local 'structure' of the turbulent flame. We compare the local turbulent flame profiles with the steady unstrained or strained one-dimensional laminar flame profile for the same chemistry and fluid properties. Of particular interest is the distribution along the flame of the normalized local flame speed ('flamelet speed') s_n defined as the integral of the heat-release profile in a direction locally normal to the flame. The local heat-release rate $\dot{\omega}_Q$ is defined by

$$\dot{\omega}_Q = \sum_{\alpha=1}^{N_s} \dot{\omega}_\alpha \Delta h_{f\alpha}^0, \tag{20}$$

and the normalized flamelet speed is then

$$s_n = \int \dot{\omega}_Q \, \mathrm{d}n \Big/ \left(\int \dot{\omega}_Q \, \mathrm{d}n \right)_0. \tag{21}$$

A normalized flame length $\mathscr{L}^*$ and turbulent flame speed s_T^* are defined as

$$\mathscr{L}^* \equiv L_{flame}/L_{flame\,0}, \tag{22}$$

$$s_T^* \equiv \overline{\dot{\omega}_Q}/\overline{\dot{\omega}_{Q0}} = \langle s_n \rangle \mathscr{L}^*. \tag{23}$$

In (21)–(23), the subscript 0 denotes the value for the unstrained planar laminar flame; overbars denote volume (area) averages while angled brackets are reserved for flame-area-weighted means (length-weighted in two spatial dimensions). A check of self-consistency is to verify the equality between s_T^* calculated in the two ways given in (23): they are found to agree to within a few percent in all cases. Note that this approach implicitly neglects curvature effects on $\dot{\omega}_Q$. Therefore (23) is rigorous only in the framework of flamelet models where it is assumed that $\dot{\omega}_Q$ is only a function of n.

3.3. *Stretched laminar flame computations – construction of a flamelet library*

In order to compare the local turbulent flame speed to that of laminar strained flames, we have performed calculations for low-Mach-number premixed laminar flames formed by a counterflow of diluted hydrogen–oxygen–nitrogen mixture and hot products as shown in figure 3.

The configuration is described by invoking a boundary-layer approximation. The governing equations along the stagnation streamline (y-axis) are written by assuming constant pressure gradient along the normal direction:

$$\frac{1}{x}\frac{\partial p}{\partial x} = \left(\frac{1}{x}\frac{\partial p}{\partial x}\right)_{\pm\infty}. \tag{24}$$

The system of equations is then obtained by writing $u(x, +\infty) = \psi x$ and $u(x, -\infty) = \psi x[(\rho_{+\infty})/(\rho_{-\infty})]^{1/2}$ and by introducing a similarity function $U(y) = u/u(x, +\infty)$, where ψ denotes the strain rate at infinity and $\rho_{+\infty}$ and $\rho_{-\infty}$ are densities in fresh gases and hot gases respectively. For more details see Darabiha *et al.*
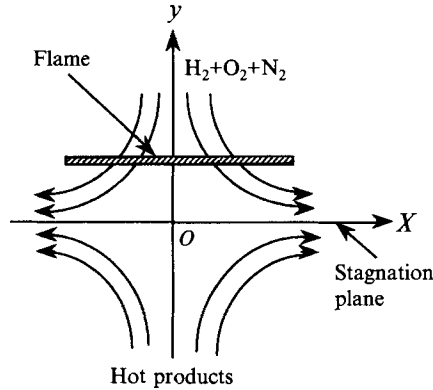
FIGURE 3. Configuration of the counterflow flame calculations. Fresh gases in the upper part are separated by the stagnation plane from burnt gases in the lower part.
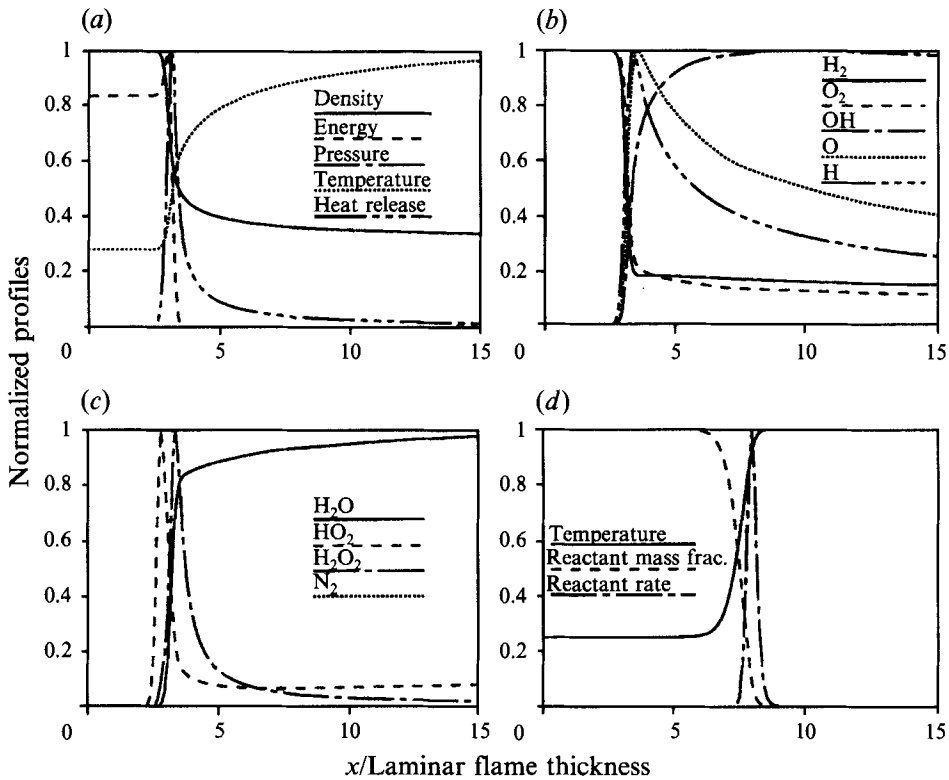

FIGURE 4. Steady unstrained laminar flame profiles: (*a–c*) H_2–air, complex chemistry, equivalence ratio $\Phi = 1.0$, unburnt gas temperature $T_u = 800$ K (cases 1, 2, 3, tables 2, 3); (*d*) one-step chemistry $\dot{w} = A\rho Y \exp([-\beta(1-\Theta)]/[1-\alpha(1-\Theta)])$, $\Theta = (T-T_u)/(T_b-T_u)$ (Haworth & Poinsot 1992).

(1989). These equations are completed by the perfect-gas state law and by formulae expressing thermochemical properties. As for DNS calculations, vectorized CHEMKIN and TRANSPORT packages (Darabiha *et al.* 1989) are used to calculate these properties. The solution procedure for this system of equations employs a pseudo-arclength continuation method and adaptive gridding. We refer to Smooke (1982), Giovangigli & Smooke (1987*a*, *b*, 1988) and Darabiha *et al.* (1989) for this method.
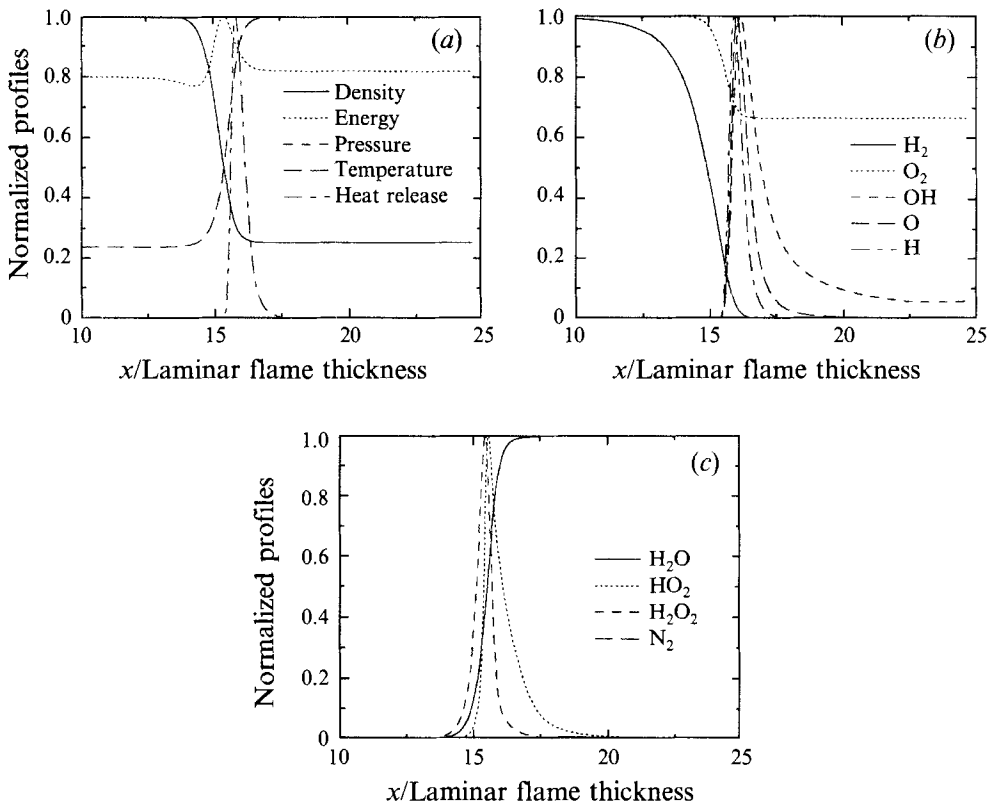
FIGURE 5. Steady unstrained laminar flame profiles: H_2–air, equivalence ration $\Phi = 0.35$, unburnt gas temperature $T_u = 300$ K (case 10, tables 2, 3).

Solving the above system for different values of the equivalence ratio and strain rate permits the construction of a library of laminar flames for use in 'flamelet' models.

A technical problem arises in the definition of the reference strain rate. In the DNS diagnostics, the local turbulent strain rate a_t is calculated at the flame front where the density ρ is different from the fresh mixture density $\rho_{+\infty}$. This strain rate a_t is not equal to ψ: these two quantities are related through: $\psi = a_t(\rho/\rho_{+\infty})^{1/2}$. We have chosen to use a_t as the reference strain rate (although ψ would also be a valid choice). Therefore, for comparison with the DNS data we corrected the strain rate of the stagnation-point flames by a factor of $(\rho_{+\infty}/\rho)^{1/2}$.

4. Results

4.1. Laminar profiles

Two fresh-gas temperatures have been considered: 300 K (for cases 9 and 10) and 800 K (cases 1–8). Profiles of the steady one-dimensional laminar solutions for $\Phi = 1.0$, $T_u = 800$ K (cases 1, 2, 3) are displayed in figure 4(a–c) and for $\Phi = 0.35$, $T_u = 300$ K (case 10) in figure 5(a–c). There each quality has been normalized by its maximum value (profiles for laminar flames with different equivalence ratios show similar characteristics). Corresponding profiles for the one-step Arrhenius scheme used in Haworth & Poinsot (1992) are shown in figure 4(d). The abscissa is in units of the laminar flame thickness δ_l, which is of the order of the heat-release zone thickness. A
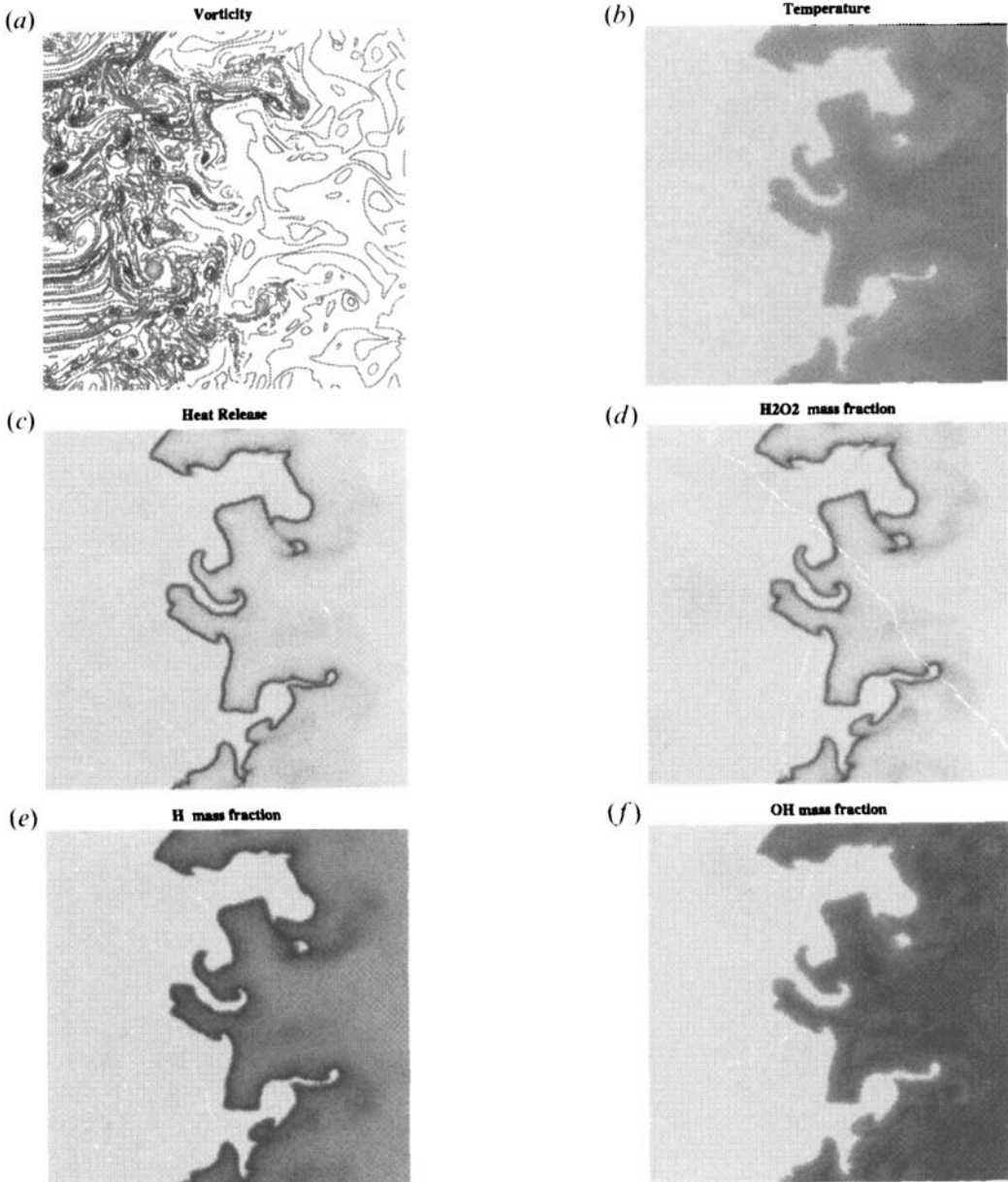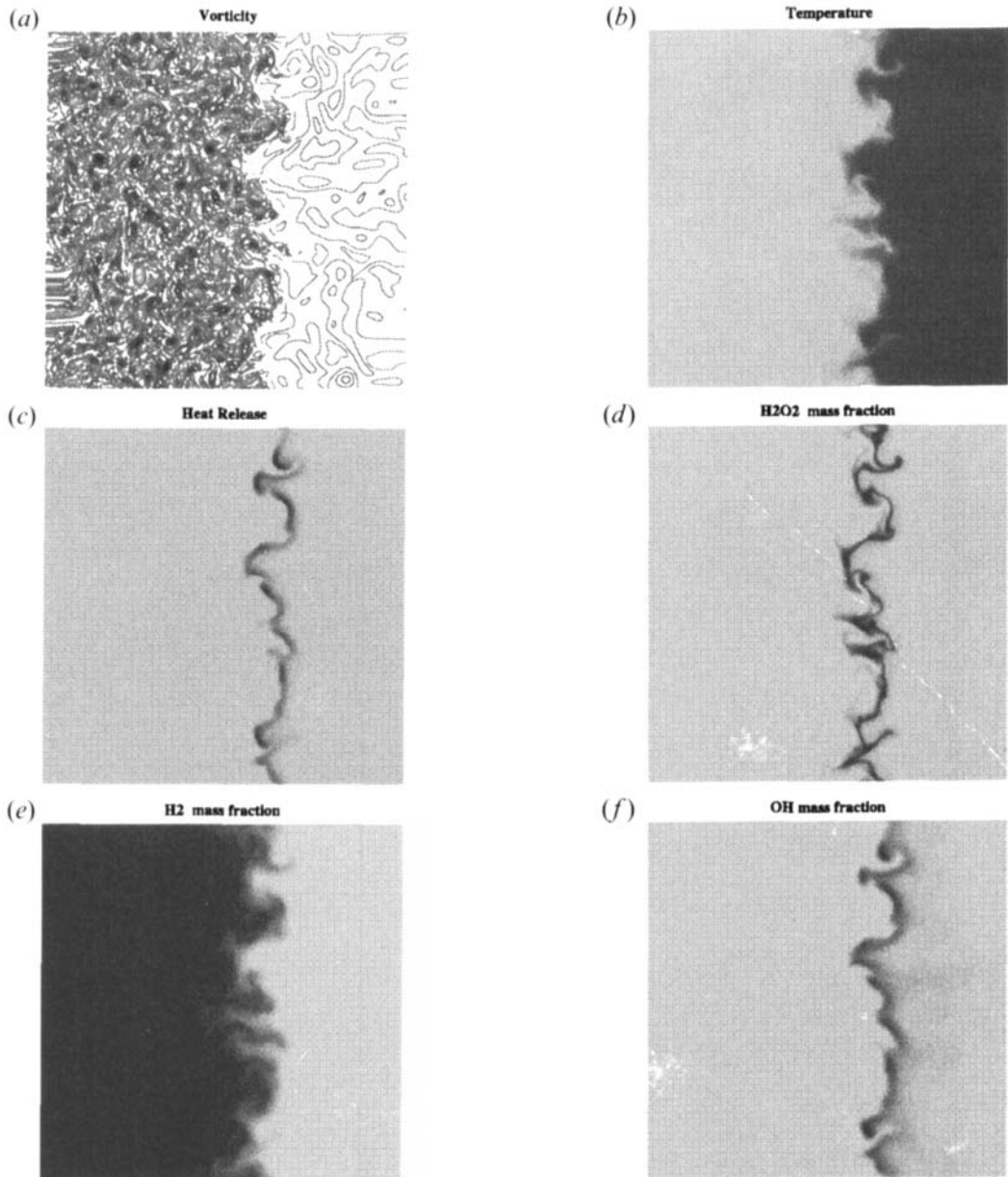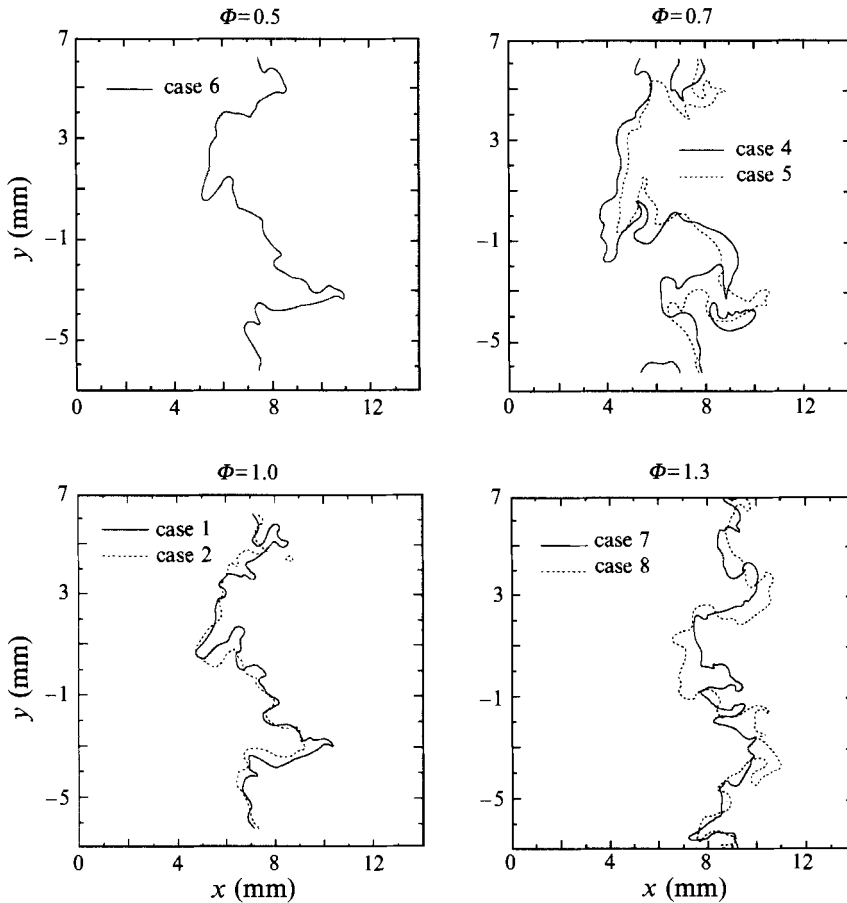
FIGURE 6. Computed fields at one instant of time, case 7, time $t/\tau_0 = 1.16$: (a) vorticity contours; (b) temperature; (c) heat release; (d) H_2O_2 mass fraction; (e) H mass fraction; (f) OH mass fraction.

striking difference between the simple- and complex-chemistry temperature and species profiles is the extended tails into the burnt gas for the complex high-temperature-chemistry case.

One might anticipate difficulty in maintaining the flame structure of figure 4(a–c) in turbulent flames; even in cases where all turbulence scales are larger than δ_l, turbulence may still be able to modify the laminar flame structure on the burnt side. Other noteworthy features of the figure 4 profiles include the significant 'leakage' of fuel and oxidizer into the products, high OH concentrations in the burnt gas, and locations of

FIGURE 7. Computed fields at one instant of time, case 10, time $t/\tau_0 = 1.0$: (a) vorticity; (b) temperature; (c) heat release; (d) H_2O_2 mass fraction; (e) H_2 mass fraction; (f) OH mass fraction.

peak radical concentrations relative to peak heat release. The high product temperature (2840 K) is responsible for the high equilibrium H_2, O_2, and OH concentrations on the burnt side. Peak OH concentration occurs well behind the peak heat–release zone, while H- and O-atom, H_2O_2 and HO_2 peak closer to the location of peak heat release. The situation is different for leaner and cooler flames (case 10, figure 5), where the OH radical level drops rapidly behind the flame front.

FIGURE 8. Isocontours $Y_{O_2} = 0.22$ at $t/\tau_0 \approx 1.0$.

4.2. *Turbulent flame contours*

Examples of computed fields at one instant of time for case 7 at $t/\tau_0 = 1.16$ and case 10 at $t/\tau_0 = 1.0$ are given in figures 6 and 7 (unburnt gases are on the left, burnt products are on the right). The initially planar flame has been severely distorted by the turbulence by this time, even to the extent of tearing off pockets of fresh gas which are carried into the product side. Eventually these pockets of fresh gas are consumed for these adiabatic flames. Nevertheless, the structure of the underlying laminar flame remains readily recognizable. Heat-release contours (figure 6c) suggest a thin flamelet-like structure albeit with some islands of fresh gas burning enveloped by the hot products. Some radicals including H_2O_2 (figure 6d) show similar behaviour to the heat release: profiles remain thin and appear to mark the region of maximum heat release. On the other hand, H-atom levels (figure 6e), while peaking close to the maximum heat-release zone, show a long diffuse tail on the burnt side, presumably a consequence of the high H diffusivity. Gradients in OH mass fraction are steep through the region of maximum heat release (figure 6f) but peak OH occurs well behind the flame front and isocontours of high OH concentration do not remain connected on the burnt side. Most of these features might be anticipated from figure 4 (a–c). Thus in the present case 7, OH does not serve as a good marker of the region of maximum heat release in the
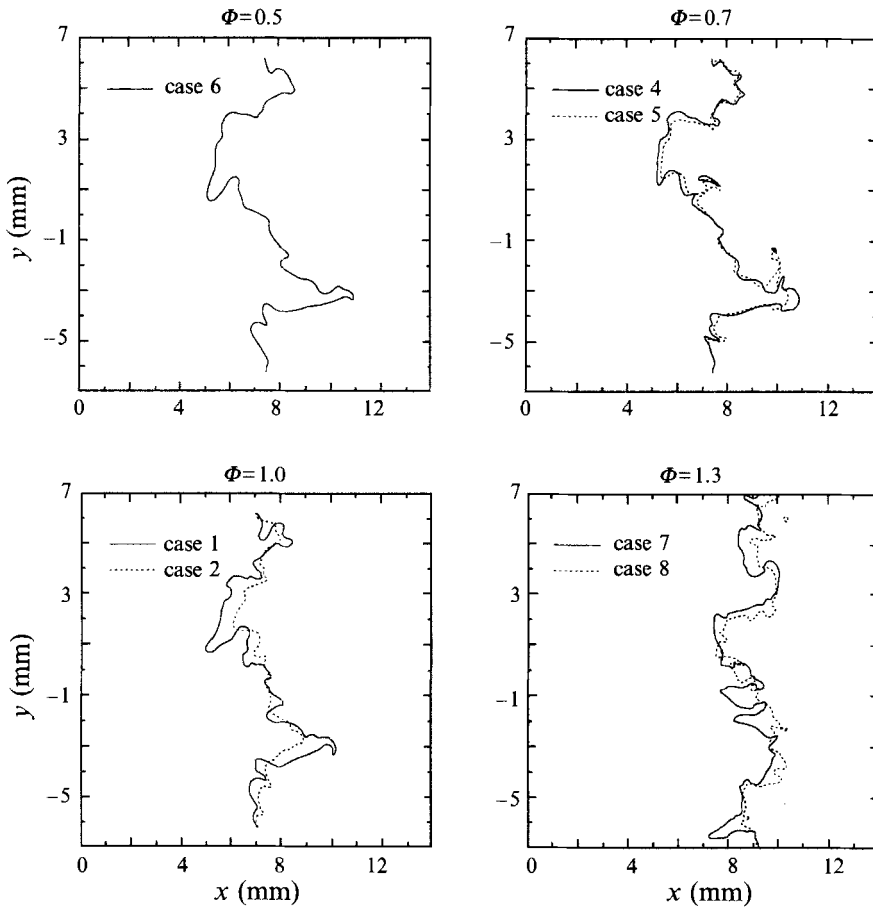
FIGURE 9. Isocontours $Y_{O_2} = 0.22$ at $t/\tau_f \approx 1.0$.

flame. For case 10, the situation is different and OH radicals follow the flame zone more closely (figure 7).

Examples of the influence of turbulence parameters on flame structure are given in figures 8 and 9. There the isocontour used to define the flame at one instant of time is plotted for several cases at equal flame times $t/\tau_f = 1.0$ and at equal turbulence times $t/\tau_0 \approx 1.0$ ($\tau_0 = \tau(t = 0)$). The cases 4, 1, 8, characterized by higher Reynolds numbers than cases 5, 2, 7 respectively, yield more highly fine-scale wrinkled flames (which eventually show pockets as in figure 6), whereas the large-scale folding is similar. This seems to be a consequence of the fact that the initial turbulence spectra are based on roughly the same scale for the most energetic vortices, whereas the Kolmogorov scale is adjusted to meet the turbulence level indicated in table 3.

4.3. Statistics of flame curvature and strain rate

Statistics of tangential strain rate and flame curvature are presented in figures 10–13. The evolution of the mean and r.m.s. values of tangential strain and curvature are displayed in figures 10 and 12 respectively. Both evolutions rapidly reach a statistically steady state (after $t/\tau_F = 0.2$). Probability density functions (p.d.f.'s) of flame tangential strain rate and flame curvature are given in figures 11 and 13, respectively. Figure 11 confirms the findings of several earlier studies using zero- and single-step chemistry
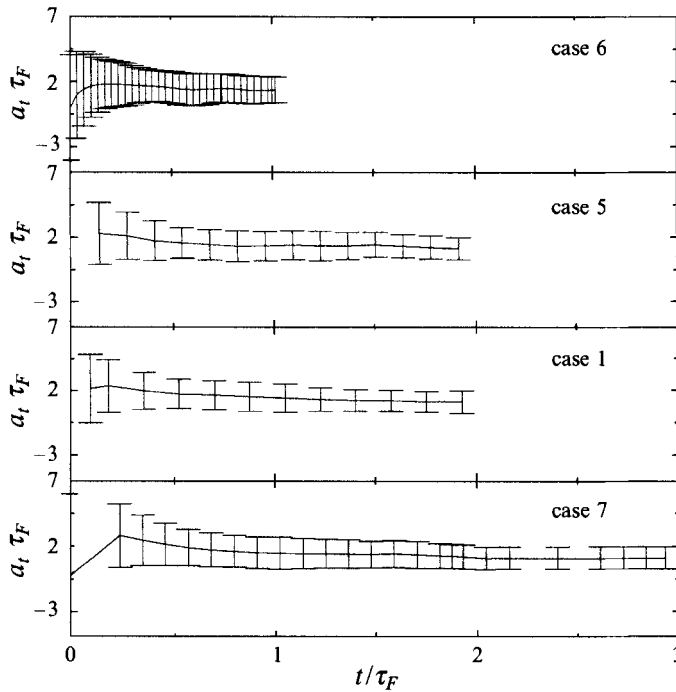
FIGURE 10. Evolution of the flame-area-averaged mean and r.m.s. of tangential strain rate; $u'/s_l^0 \approx 2.7$, $l/\delta_l \approx 2.9$. The mean value is traced with error-bars indicating its r.m.s.
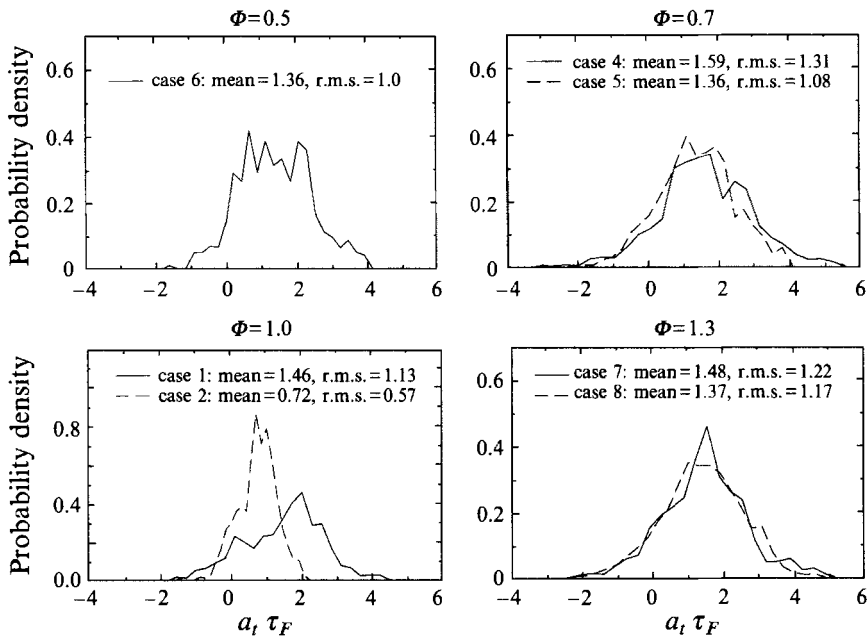
FIGURE 11. P.d.f.'s of normalized tangential strain rates, $t/\tau_f = 1.0$.

models: the turbulent flame aligns preferentially with extensive strain rates in the tangent plane (Ashurst 1990; Girimaji, & Pope 1992; El Tahry *et al.* 1991; Cant *et al.* 1990; Rutland *et al.* 1990; Rutland & Trouvé 1990). Figure 13 also is reminiscent of results found using simpler models (Haworth & Poinsot, 1992) and experiments (Lee,
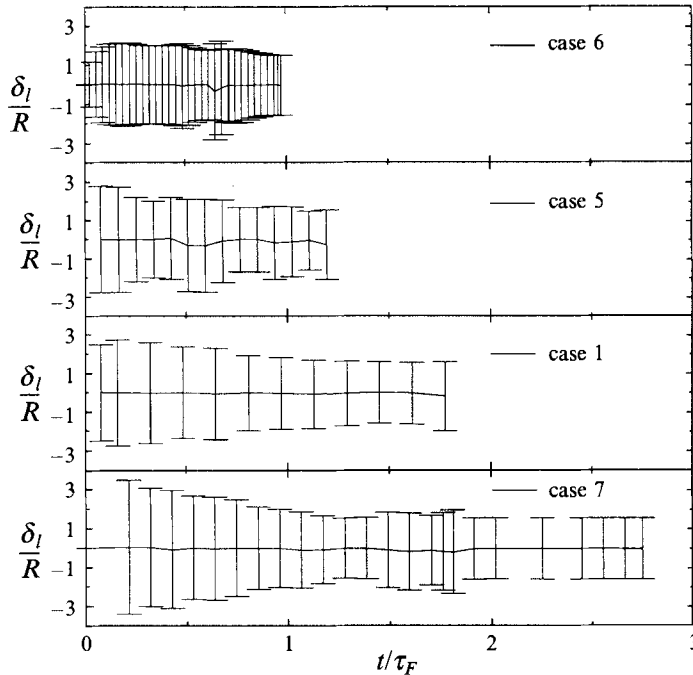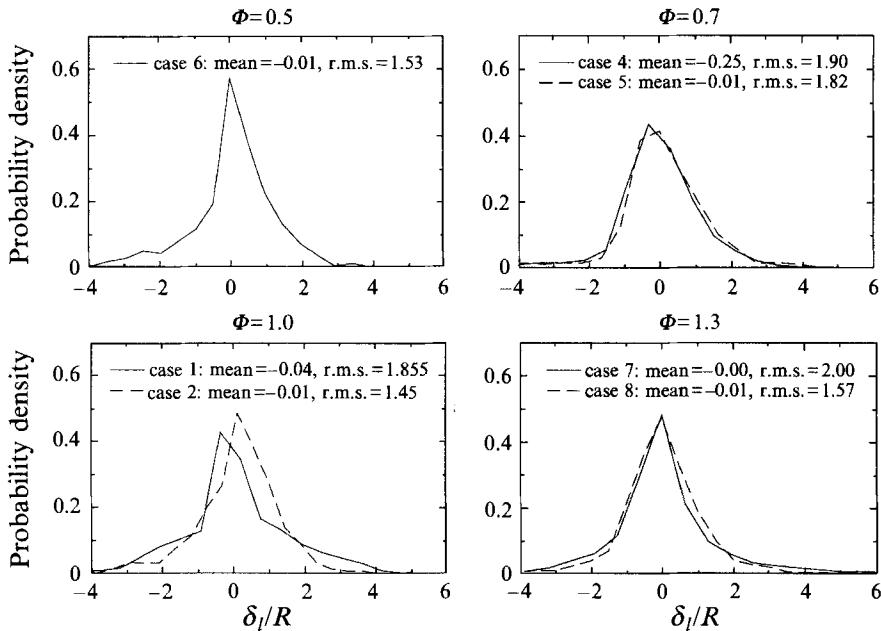
FIGURE 12. As figure 10 but for normalized flame curvature.

FIGURE 13. P.d.f.'s of normalized flame curvature, $t/\tau_0 = 1.0$.

North & Santavicca 1992): curvature p.d.f.'s are close to symmetric with near-zero mean curvature. While some skewing of the p.d.f.'s towards negative curvature might be expected at low u'/s_l^0 (Rutland *et al.* 1990; Becker *et al.* 1990), no such skewing is evident here. The more highly wrinkled nature of the flames of cases 1, 4, 7, 8 is manifested in the broader tails (higher r.m.s.) of their curvature p.d.f.'s. The minimum
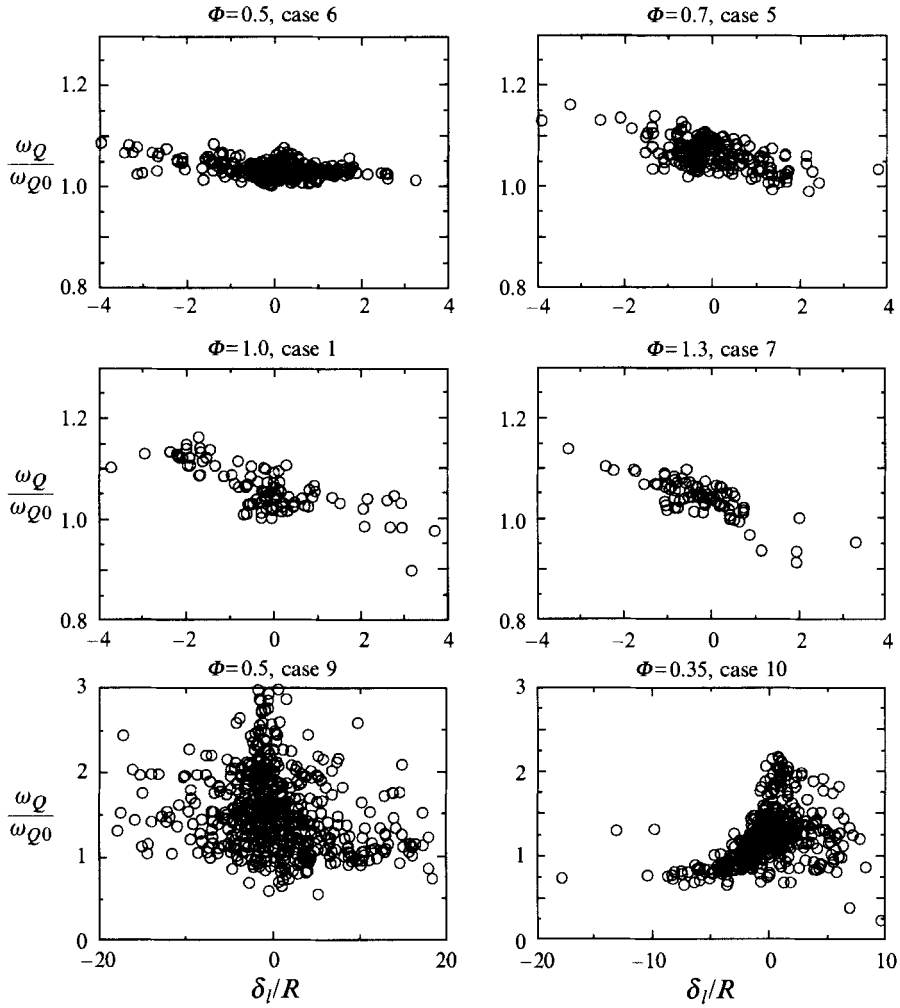
FIGURE 14. Scatter plots of normalized maximum heat release $\dot{\omega}_{Q,max}/\dot{\omega}_{Q0,max}$ (equation (20)) versus normalized flame curvature at $t/\tau_0 \approx 1.0$: cases 6, 5, 1, 7, $u'/s_l^0 \approx 2.7$, $l/\delta_l \approx 2.9$, cases 9, 10, $u'/s_l^0 \approx 30$, $l/\delta_l \approx 1.3$.

radius of curvature obtained here is of the order of a quarter of the flame thickness ($\mathcal{R}/\delta_l = 0.25$). This is slightly less than the values obtained for simple-chemistry computations (Haworth & Poinsot 1992) in which minimum radii of curvature were close to half the flame thickness.

4.4. *Statistics of maximum heat release*

Figures 14 and 15 provide correlations between local maximum heat release ($\dot{\omega}_{Q,max}/\dot{\omega}_{Q0,max}$) and curvature and strain. Each point in these figures corresponds to a point sampled uniformly along the isocontour defining the turbulent flame. The local maximum heat release appears to correlate with curvature (figure 14), but not with strain: maximum heat release decreases with increasing curvature for flames where the equivalence ratio $\Phi > 0.5$ (cases 1, 2, 3, 4, 5, 7, 8), and the slope of the correlation increases in magnitude with equivalence ratio. For leaner and cooler flames ($\Phi = 0.35$) the correlation is inverted: maximum heat release increases with increasing curvature,
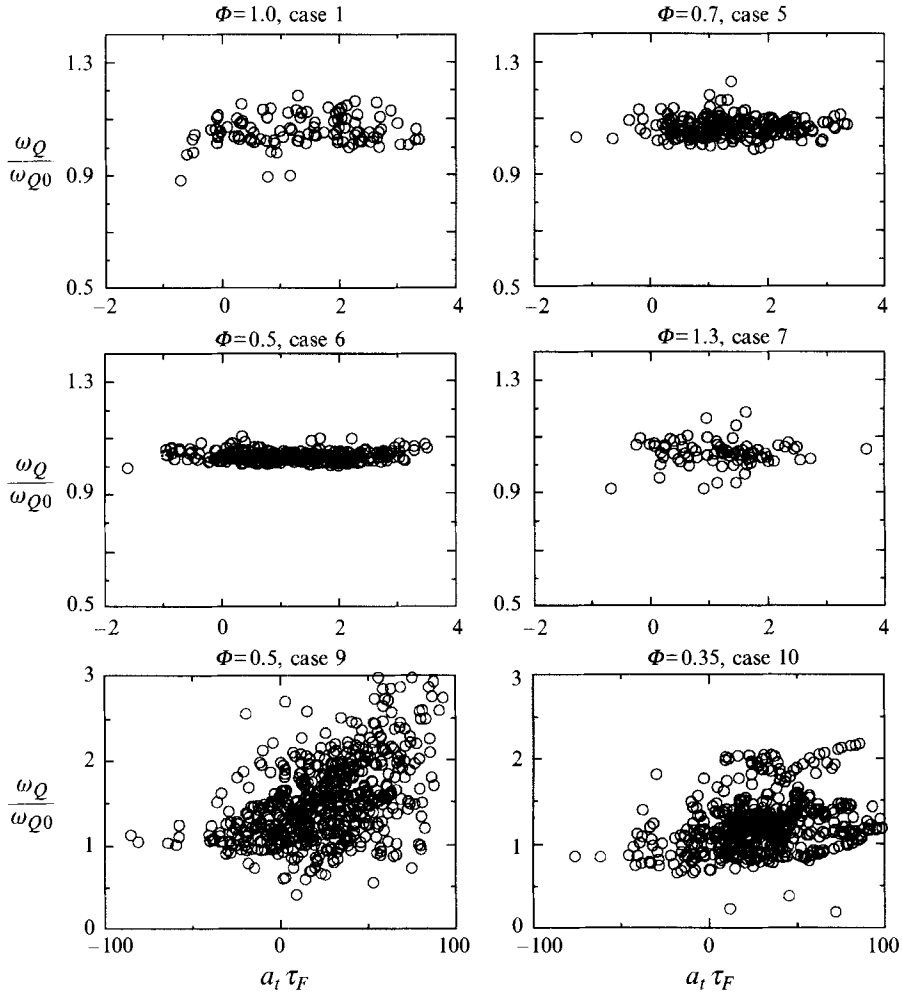
FIGURE 15. As figure 14, but for tangential strain rate.

and the slope of the correlation decreases in magnitude with equivalence ratio. These results are consistent in view of the findings in Haworth & Poinsot (1992) for simple chemistry in the sense that curvature dominates the local flame structure. However, Haworth & Poinsot (1992) report local reaction rates that increase with increasing curvature for $Le < 1$ and that decrease with increasing curvature for $Le > 1$. Thus figure 14 suggests that the 'equivalent' Lewis number for these flames is more than unity for $\Phi > 0.5$ and less than unity for $\Phi < 0.5$. Asymptotic analysis (Garcia-Ybarra, Nicoli & Calvin 1984) suggests that correlations between curvature (or strain) and heat release are controlled by a Markstein length. This length is a function of various chemical parameters including the Lewis number. Note that different Markstein lengths have to be used depending on whether one considers the flame displacement speed or the flame consumption speed (integrated reaction rate) (Clavin & Williams 1982). Moreover Markstein lengths obtained by experiments or asymptotic analysis do not compare well for hydrogen/air flames (Kwon, Tseng & Faeth 1992; Searby & Quinard, 1990). For example in the experimental condition of Kwon et al., it is found that the Markstein length changes sign around an equivalence ratio of $\Phi = 1.4$, while
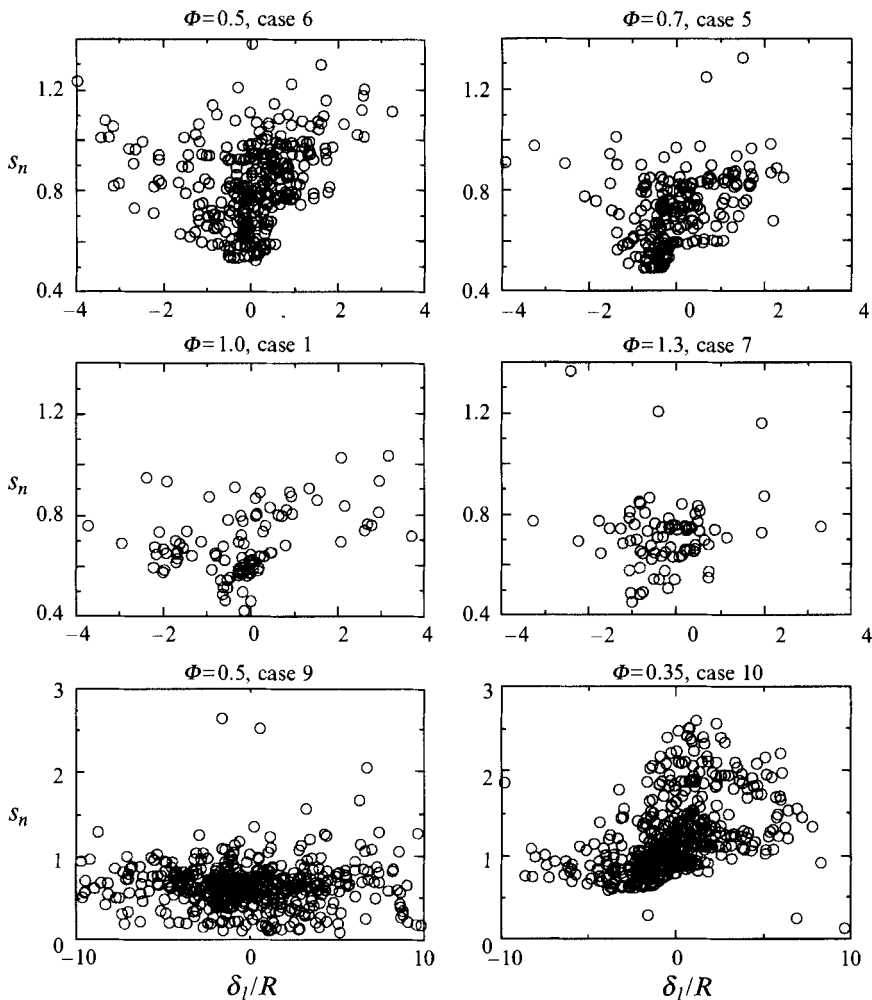
FIGURE 16. Scatter plots of normalized flamelet speed s_n (equation (21)) versus normalized flame curvature at $t/\tau_0 \approx 1.0$: cases 6, 5, 1, 7, $u'/s_l^0 \approx 2.7$, $l/\delta_l \approx 2.9$, cases 9, 10, $u'/s_l^0 \approx 30$, $l/\delta_l \approx 1.3$.

estimates based on asymptotic analysis (Garcia-Ybarra *et al.* 1984) suggests a value of 1.06.

Clearly, the definition of Lewis number is problematic in a multicomponent system. While the fuel-based (H_2) Lewis number in the present case is less than unity, a Lewis number can be defined for each species and these Lewis numbers will be spatially non-uniform. It has been argued (Chelliah & Williams 1987) that away from stoichiometric, the most relevant Lewis number influencing overall reaction rate is the Lewis number based on diffusion of the limiting (deficient) reactant into the reaction zone. By this analysis, we would expect to see results qualitatively similar to simple chemistry with $Le < 1$ for the present $\Phi < 1$ cases, and results similar to simple chemistry with $Le > 1$ for the present $\Phi > 1$ cases. This description does not match the observed DNS results.

A different analysis by Joulin & Mitani (1981) leads to the definition of an 'equivalent Lewis number' governing the global behaviour of premixed flames with complex chemistry. Equivalent Lewis numbers for the H_2–O_2 system vary from 0.38 for $\Phi = 0.5$ to 0.94 for $\Phi = 1.3$, according to this analysis. In this case, we should expect
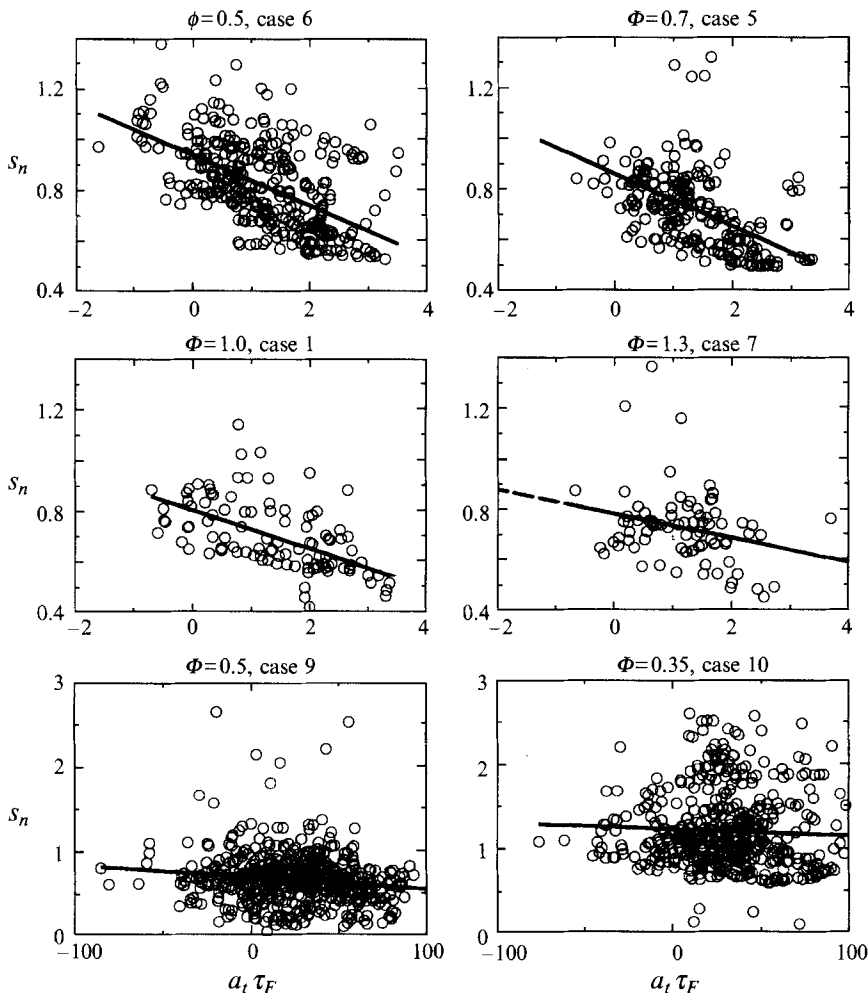
FIGURE 17. As figure 16 but for normalized tangential strain rate. Linear least-square fits show the general tendencies.

to see results similar to the simple-chemistry $Le < 1$ results at all equivalence ratios in the present study. This again is not observed in the DNS results.

Inconsistencies between the present complex-chemistry results and earlier simple-chemistry simulations and theories based on equivalent global Lewis numbers suggest that the local flame structure in real flames is not governed only by diffusion of heat and reactants into the reaction zone. Complex-chemistry effects such as radical diffusion and shifts in peak radical concentration may be important. Transition from an equivalent Lewis number $Le > 1$ behaviour to a $Le < 1$ behaviour is indeed observed but the threshold corresponds to an equivalence ratio $\Phi \approx 0.5$. The influence of the flame temperature has not been studied in detail here, but has also to be considered.

4.5. Statistics of flamelet consumption speed

Scatter plots of local flamelet speed s_n versus local flame curvature and local tangential strain rate are given in figures 16 and 17, respectively. These results are different from the correlations obtained for the maximum heat release (figures 14 and 15): for most
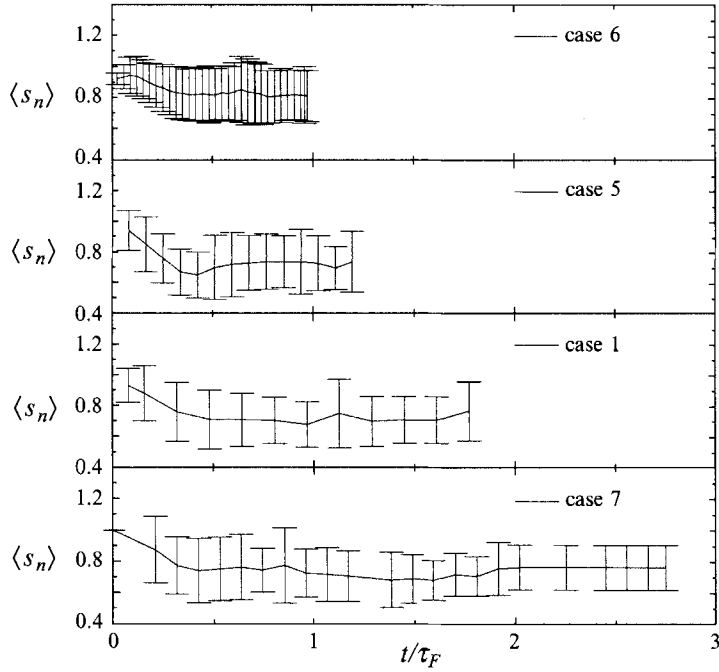
FIGURE 18. Evolution of the flame-area-averaged mean and r.m.s. of normalized flamelet speed s_n: $u'/s_l^0 \approx 2.7$, $l/\delta_l \approx 2.9$. The mean value is traced with error-bars indicating its r.m.s.
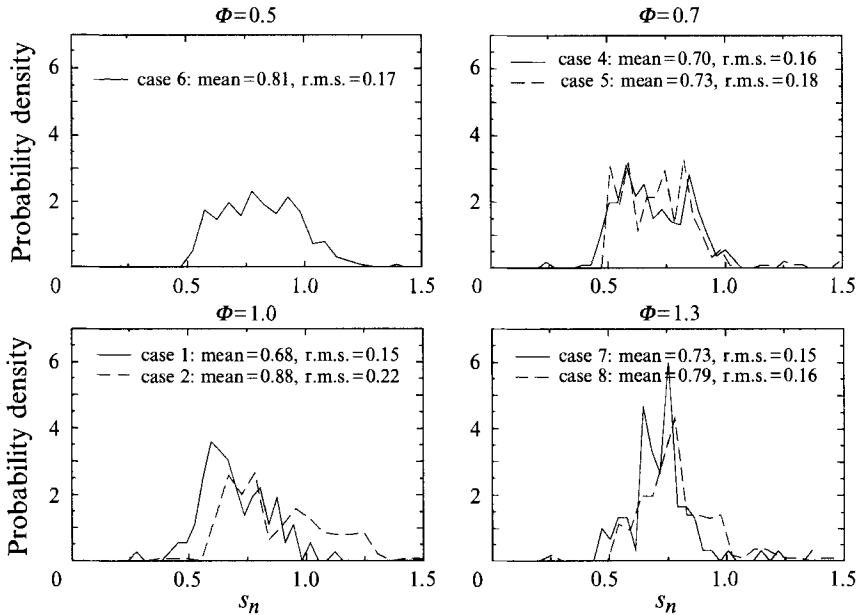

FIGURE 19. P.d.f.'s of normalized flamelet speed s_n (equation (21)), $t/\tau_0 = 1.0$.

cases (1–8) no correlation of local burning velocity with curvature is evident and the decrease in s_n with increasing tangential strain rate is surprisingly strong. For case 10, however, the flame is clearly in an unstable condition as described by Haworth & Poinsot (1992) for simple-chemistry and $Le < 1$ cases. The flamelet speed increases
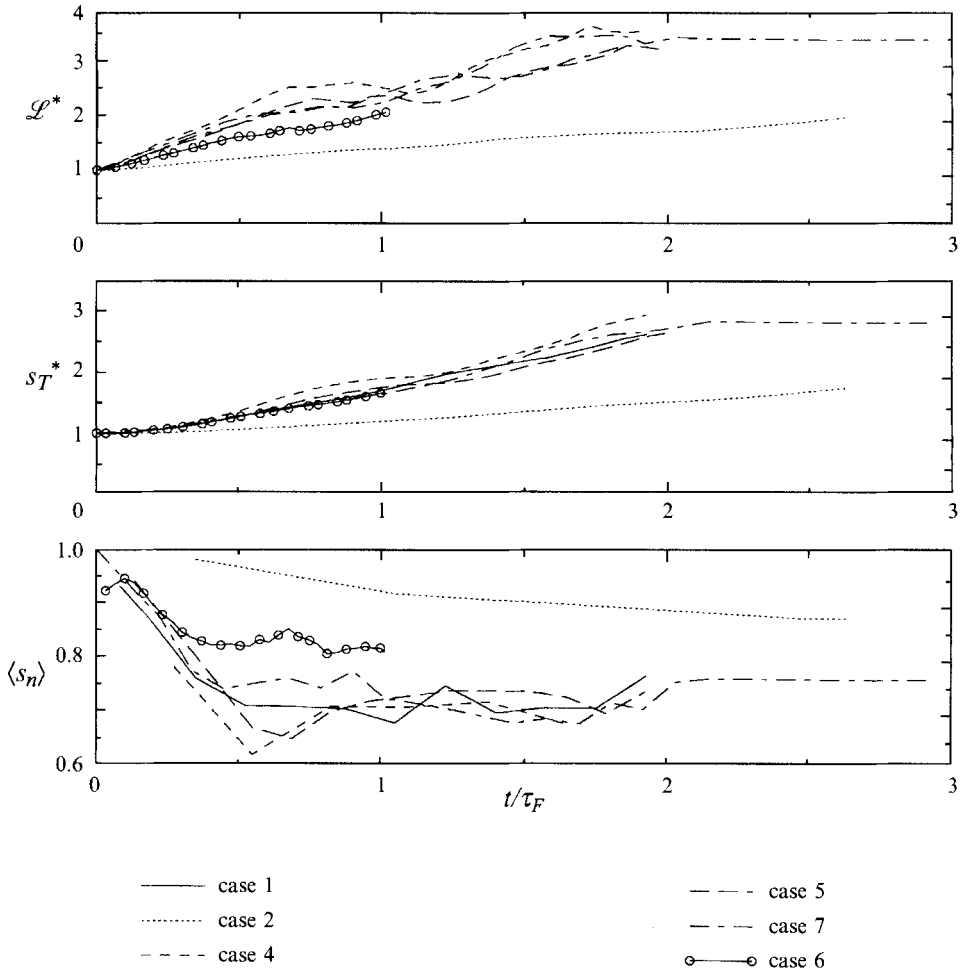
FIGURE 20. Evolution with time of flame-area-averaged normalized flamelet speed $\langle s_n \rangle$ (equation (21)), normalized flame area $\mathscr{L}^*$ (22), and normalized turbulent flame speed s_T^* (23).

with positive curvature and can reach values up to $2.5s_l^0$. This transition is very violent and confirms that very lean H_2–O_2 turbulent flames exhibit instabilities and are quite different from richer flames as observed in experiments (Becker *et al.* 1990; Lee *et al.* 1993; Wu *et al.* 1990).

Figure 18 portrays the evolution of the flame-area-averaged normalized mean flamelet speed $\langle s_n \rangle$ and its r.m.s. for four cases of different equivalence ratio and similar turbulence parameters (equal u'/s_l^0 and l/δ_l). From the initial delta-function p.d.f. at a mean value of 1.0 the mean flamelet speed and the flamelet speed where the p.d.f. peaks (figure 19) decrease to a statistically steady state, while the r.m.s. is broadening from 0 to stable values. Examples of the p.d.f.'s of the mean flamelet speed are given in figure 19. The cases 1, 4, 7, characterized by higher turbulence levels than cases 2, 5, 8 respectively, show lower mean and r.m.s. values. While the cases $\Phi = 1.0$ and 1.3 show a clear peak in the flame speed p.d.f., the cases $\Phi = 0.5$ and 0.7 are characterized by a flat (rectangular) p.d.f. The characteristics of the flamelet speed reach a statistically steady state in a rather short time ($t/\tau_F < 1.0$), while the increase in flame area does not reach a steady state by the end of the simulations except for case 7 (figure 20). Flame area $\mathscr{L}^*$ appears to be more sensitive to turbulence parameters

than to thermochemistry (equivalence ratio). The evolution in figure 20 suggests that the normalized turbulent flame speed s_T^* depends essentially on u'/s_l^0.

While the mean consumption rate per unit area of flame $\langle s_n \rangle$ (see (21)) is significantly smaller than unity, the increase in flame area $\mathscr{L}^*$ (see (22)) more than compensates to yield normalized turbulent flame speeds s_T^* (see (23)) that are greater than unity, as expected. As shown in the previous section peak heat-release rates increase in all cases compared to the laminar flame. For this reason the reduction of local consumption rate $\langle s_n \rangle$ must be primarily a flame thickness effect.

These results are unexpected in view of the findings in Haworth & Poinsot (1992) for simple chemistry. There it was found that a correlation between local burning velocity and local tangential strain rate was evident only for $Le = 1$ and that this correlation was rather weak. In no case was the straining sufficiently high to yield the extremely low values of $\langle s_n \rangle$ found here with complex chemistry. The picture provided by the present simulation is more consistent with the classical idea of flamelet models in which strain only controls the flame speed. The difference observed between results obtained with simple chemistry and with complex chemistry may be explained by investigating the local flame structure in more detail.

4.6. *Local flame structure*

Profiles of heat-release rate, temperature and OH mass fraction along the local flame normal are overlaid on the corresponding laminar profiles in figure 21 for case 7 at $t/\tau_F = 2.37$. The turbulent profiles have been uniformly sampled along the turbulent flame front; only a limited number of turbulent profiles is shown, for clarity. At early times (not shown) local turbulent profiles collapse neatly onto the unstrained laminar flame contours. Later (figure 21) the collapse remains reasonable on the fresh-gas side while turbulent profiles generally shift inwards towards the peak heat-release zone on the burnt-gas side. This results in somewhat steeper profiles and shorter tails for temperature and species profiles, whereas the maximum of the heat-release profile is increased compared to the profile of the steady laminar flame. This appears to a be a consequence of the net extensive tangential strain rates thinning the flame in the turbulent flow and reducing the local flamelet speed while peak heat release rate increases. Similar results are obtained for all equivalence ratios.

4.7. *Using the OH radical to characterize the flame front*

Levels of OH radicals have been used in many studies to infer information on the local behaviour of combustion (Hurle *et al.* 1968; Poinsot *et al.* 1987; Becker *et al.* 1990). From the present results we can quantitatively assess the limits of this assumption in turbulent flames. First the high adiabatic flame temperature (2840 K) used in cases 1–8 leads to significant levels of OH in the burnt gases and OH is a poor marker of the heat-release zone in these cases. No correlation can be found between OH levels and reaction rates (figure 6).

If cooler reactants are used (cases 9 and 10) OH radical mass fraction follows the flame front more closely (figure 7). In this case it is possible to make two important observations:

(i) The maximum OH level along the flame front correlates with curvature: higher OH levels are found in regions of positive curvature (figure 22*d*). This correlation is the one expected from previous simple-chemistry studies for $Le < 1$. These results also are consistent with experimental observations by Lee *et al.* (1993) and Becker *et al.* (1990) in lean hydrogen–air flames: OH levels are higher in flame elements concave towards the burnt gases.
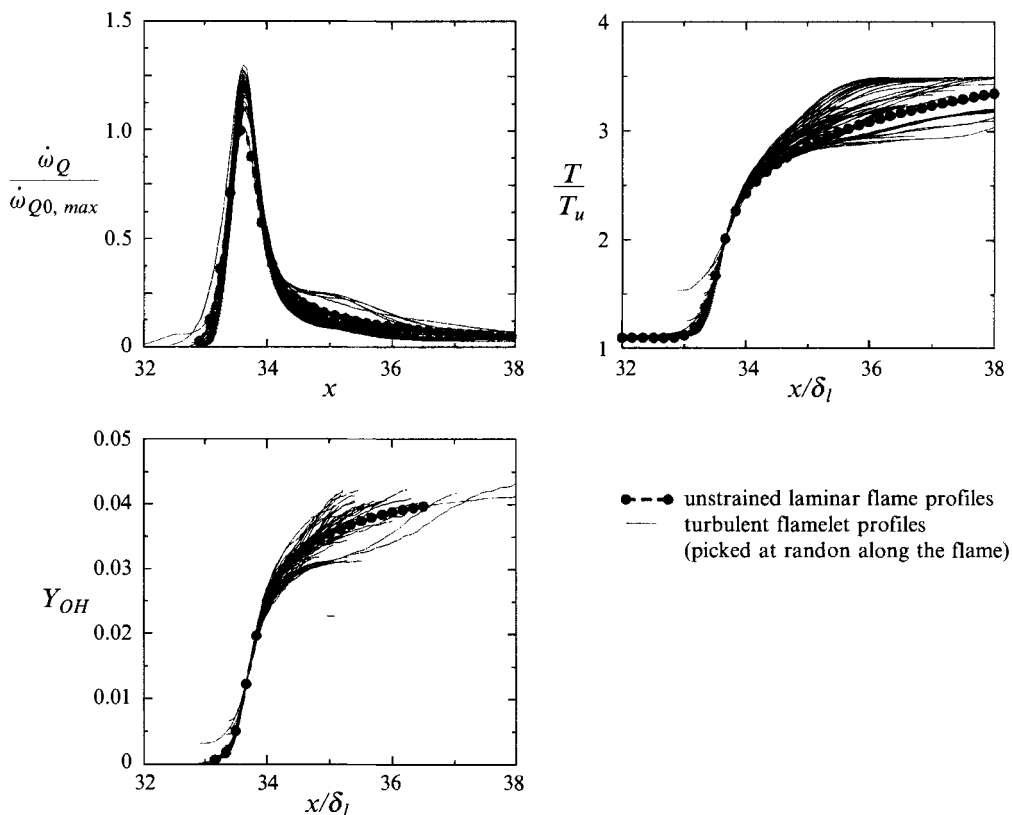
FIGURE 21. Laminar and turbulent flame profiles for case 7: $\phi = 1.3$; $t/\tau_F = 2.37$; $t/\tau_0 = 2.23$.

(ii) A weak correlation between the flamelet speed s_n and the local maximum OH level exists for $\Phi = 0.35$ (figure 22e, case 10) as well as for $\Phi = 0.5$ (figure 22b, case 9). Such a correlation is used by Becker et al. (1990) to deduce flame speeds s_n from OH measurements, assuming $s_n \sim$ [OH]. In the same way, maximum reaction rates are also correlated with maximum OH levels (figure 22f). These results show that the OH radical may be a good marker of the reaction mechanisms in turbulent flames but only for lean and cool flames (cases 9 and 10) and only with a rather large error margin. In other situations (cases 1–8) OH cannot be used to characterize combustion. Clearly the H_2O_2 radical would better serve in this regard computationally, but may be a poor choice in practice: peak H_2O_2 mass fraction in the present $\Phi = 1.0$ flame (case 3) is 0.000094 versus 0.0348 for OH. Moreover, the reaction-rate constants involving H_2O_2 in table 1 are not well established.

5. Validity of the 'flamelet-library' approach

An important result obtained above is that the turbulent flamelets in the present simulations 'qualitatively' follow the classical flamelet assumption: the local flame speed is controlled mainly by strain. In this section we address the question of whether the flamelet assumption holds quantitatively: i.e. does the flamelet speed predicted using a steady stagnation-point flame computation with a prescribed strain rate match the local flame speed for a turbulent flame element experiencing the same instantaneous
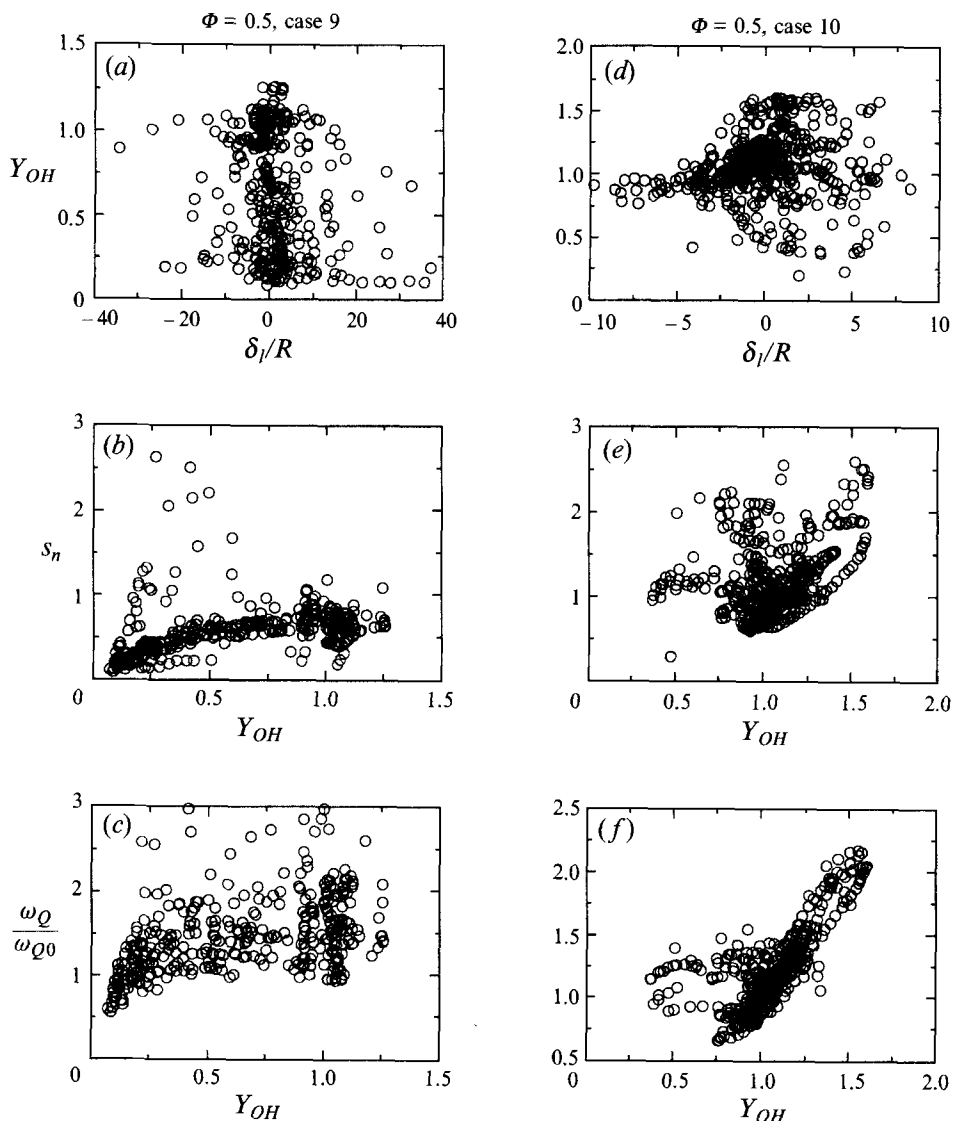
FIGURE 22. Scatter plots of the maximum level of OH along the normal to the flame and the curvature (a, d) of the maximum reaction rate (c, f), and of the flamelet consumption speed (b, e) with OH. OH mass fractions are normalized by their maximum in the corresponding unstrained laminar flame. Results are for the cooler and leaner flames cases 9 and 10.

strain? To check this, 'flamelet libraries' have been computed by the method outlined in §§3.3 for $\Phi = 0.5$, 1.0, 1.3. The resulting relationships between flame speed and strain rate are shown in figure 23 (stable solutions for strained planar flames cannot be obtained for $a_t < 0$). For these steady flames (cases 1, 6, 7) the laminar flame speed first increases with increasing strain rate a_t, reaching a maximum for $a_t \tau_F \approx 0.2$, and then decreases at higher values of a_t. The situation is similar for case 9. This nonlinearity is due to large differences among species diffusion velocities. Figure 23 shows that in all situations where fresh gases are at 800 K the results given by computations of steady flames overpredict the effects of strain on the local turbulent flame speed. Unsteady effects may moderate the effects of large straining in the turbulent flames. When the
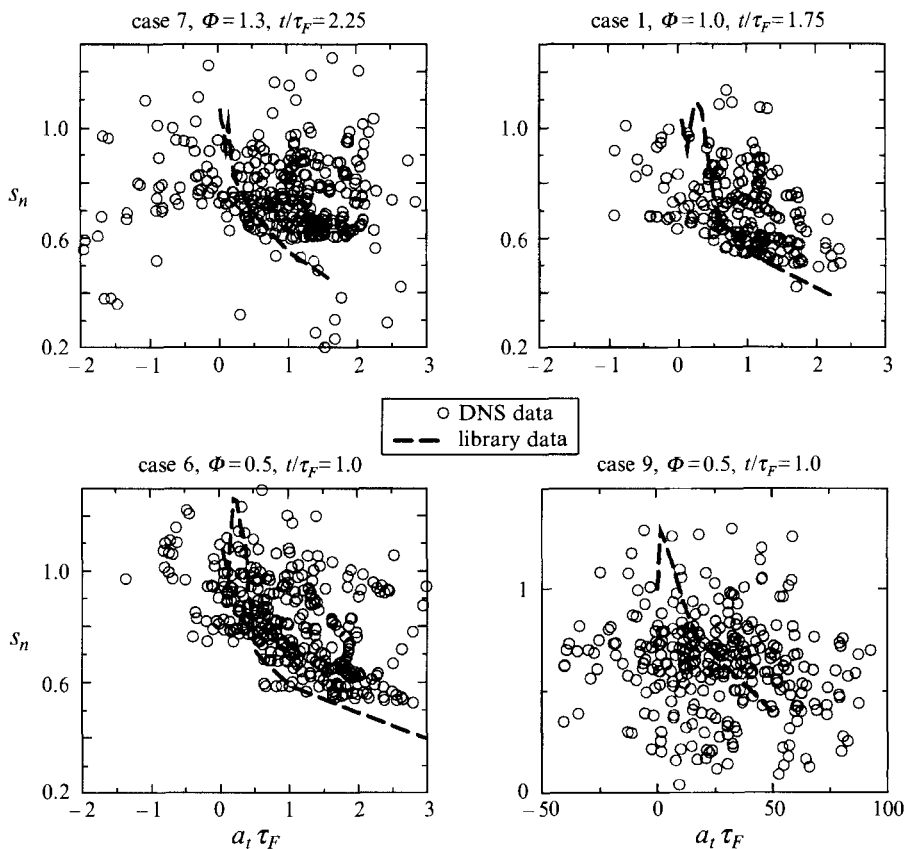
FIGURE 23. Scatter plots of normalized flamelet speed s_n versus tangential strain rate for the turbulent cases 6, 1, 7, $u'/s_l^0 \approx 2.7$, $l/\delta_l \approx 2.9$, case 9, $u'/s_l^0 \approx 30$, $l/\delta_l \approx 1.3$ and results from steady strained flame computations.

fresh gas temperature is 300 K, the correlation with the library is better, despite a large scatter of the results. In all cases the correlation is rather poor. Note also that we use strain (a_t) and not stretch $(a_t - s_d/\mathscr{R})$ in figure 23. Conclusions are similar when stretch is used.

6. Conclusions

The present simulations represent a first attempt to incorporate realistic chemical kinetics and transport into full turbulence simulations. Main results are as follows:

(i) Realistic chemical kinetics and transport have been implemented successfully into full turbulence simulations.

(ii) Consistent with the simpler models, the complex-chemistry turbulent flame aligns preferentially with extensive strain rates in the tangent plane and flame curvature p.d.f.'s are close to symmetric with near-zero means.

(iii) Local flame structure correlates with local tangential strain rate. Turbulent straining results in substantial thinning of the flame relative to the steady unstrained laminar case, while the peak heat-release rate increases with strain: integrated heat release along the local flame normal is substantially lower in the turbulent flame.

(iv) A discernable transition from fuel-lean cases $(Le < 1)$ to fuel-rich cases $(Le > 1)$

is observed as obtained in previous simple-chemistry studies (Haworth & Poinsot 1992). For very lean flames ($\Phi = 0.35$), instabilities occur and consumption speeds may grow to two to three times s_l^0. A similar transition has been observed in simple-chemistry computations, but at $\Phi = 1$ (Haworth & Poinsot 1992). For complex chemistry, transition to unstable cases occurs around $\Phi = 0.4$. This transition is also observed in the correlations of maximum reaction rates and of flame speed with curvature: the correlation changes sign when the equivalence ratio changes from very lean to rich. These results indicate that the notion of a single rate-controlling global deficient-reactant-based Lewis number is valid in turbulent flames but that other mechanisms also may play a role.

(v) In all cases investigated here, heat release and H_2O_2 contours remain thin and connected (flamelet-like). A flamelet assumption seems to be qualitatively satisfied.

(vi) The 'flamelet-library' approach does not yield quantitatively accurate results in the present cases: steady-state stagnation-point flame computations overpredict the effects of straining on the flamelets.

(vii) For high temperature of the fresh gases maximum OH levels occur far behind the flame front and cannot be used to track the flame or to characterize its consumption speed. For cooler leaner flames ($\Phi < 0.4$, $T_u = 300$ K), the OH radical may be used to estimate local reaction rate and flame speed.

REFERENCES

ASHURST, W. T. 1990 Geometry of premixed flames in three-dimensional turbulence. In *Proc. 1990 Summer Program*, pp. 245–253. Center for Turbulence Research, Stanford University and NASA Ames.

ASHURST, W. T. & BARR, P. K. 1983 Stochastic calculation of laminar wrinkled flame propagation via vortex dynamics. *Combust. Sci. Technol.* **34**, 227–256.

ASHURST, W. T., PETERS, N. & SMOOKE, M. D. 1987 Numerical simulation of turbulent flame structure with non-unity Lewis number. *Combust. Sci. Technol.* **53**, 339–375.

ASHURST, W. T., SHIVASHINSKY, G. I. & YAKHOT, V. 1988 Flame-front propagation in non-steady hydrodynamic fields. *Combust. Sci. Technol.* **62**, 273–284.

BATCHELOR, G. K. 1953 *The Theory of Homogeneous Turbulence*. Cambridge University Press.

BECKER, H., MONKHOUSE, P. B., WOLFRUM, J., CANT, R. S., BRAY, K. N. C., MALY, R., PFISTER, W., STAHL, G. & WARNATZ, J. 1990 Investigation of extinction in unsteady flames in turbulent combustion by 2D-LIF of OH radicals and flamelet analysis. In *23rd Symp. (Intl) on Combustion*, pp. 817–823. The Combustion Institute, Pittsburgh.

BLINT, R. J. 1988 Flammability limits for exhaust gas diluted flames. In *22nd Symp. (Intl) on Combustion*, pp. 1547–1554. The Combustion Institute, Pittsburgh.

BLINT, R. J. 1991 Stretch in premixed laminar flames under IC engine conditions. *Combust. Sci. Technol.* **75**, 115–128.

BOUDIER, P., HENRIOT, S., POINSOT, T. & BARITAUD, T. 1992 A model for turbulent flame ignition and propagation in spark ignition engines. In *24th Symp. (Intl) on Combustion*, pp. 503–510. The Combustion Institute, Pittsburgh.

BRAY, K. N. C. & CANT, R. S. 1991 Some applications of Kolmogorov's turbulence research in the field of combustion. *Proc. R. Soc. Lond.* A, **434**, 217–240.

CANDEL, S. M. & POINSOT, T. J. 1990 Flame stretch and the balance equation for the flame area. *Combust. Sci. Technol.* **70**, 1–15.

CANT, R. S., RUTLAND, C. J. & TROUVÉ, A. 1990 Statistics for laminar flamelet modeling. In *Proc. 1990 Summer Program*, pp. 271–279. Center for Turbulence Research, Stanford University & NASA Ames.

CHELLIAH, H. K. & WILLIAMS, F. A. 1987 Asymptotic analysis of two-reactant flames with variable properties and Stefan–Maxwell transport. *Combust. Sci. Technol.* **51**, 129–144.

CLAVIN, P. & WILLIAMS, F. 1982 Effects of molecular diffusion and of thermal expansion on the structure and dynamics of premixed flames in turbulent flows of large scale and low intensity. *J. Fluid Mech.* **116**, 251–282.

DARABIHA, N. & CANDEL, S. 1992 The influence of the temperature on extinction and ignition limits of strained hydrogen-air diffusion flames. *Combust. Sci. Technol.* **86**, 67–85.

DARABIHA, N., GIOVANGIGLI, V., CANDEL, S. & SMOOKE, M. D. 1989 Vectorized computation of complex chemistry flames. In *Proc. Intl Symp. on High Performance Computing, Montpellier, France* (ed. J. Delhaye & E. Gelenbe). Elsevier.

DIXON-LEWIS, G. & MISSAGHI 1988 Structure and extinction limits of counterflow diffusion flames of hydrogen nitrogen mixture in air. In *22nd Symp. (Intl) on Combustion*, pp. 1461–1470. The Combustion Institute, Pittsburgh.

DIXON-LEWIS, G. & WILLIAMS, D. 1979 The oxidation of hydrogen and carbon monoxide. *Phil. Trans. R. Soc. Lond.* A **292**, 45–99.

DRAKE, M. C. & BLINT, R. J. 1988 Structure of laminar opposed-flow diffusion flames with $CO/H_2/N_2$ fuel. *Combust. Sci. Technol.* **61**, 187–224.

EL TAHRY, S. H. 1990 A turbulence combustion model for premixed charge engines. *Combust. flame* **79**, 122–140.

EL TAHRY, S. H., RUTLAND, S. H. & FERZIGER, J. H. 1991 Structure and propagation speeds of turbulent premixed flames – a numerical study. *Combust. Flame* **83**, 155–173.

GARCIA-YBARRA, P., NICOLI, C. & CALVIN, P. 1984 Soret and dilution effects on premixed flames. *Combust. Sci. Technol.* **42**, 87–109.

GHONIEM, A. F. & KRISHNAN, A. 1988 Origin and manifestation of flow/combustion interactions in a premixed shear layer. In *22nd Symp. (Intl) on Combustion*, pp. 665–657. The Combustion Institute, Pittsburgh.

GIOVANGIGLI, V. & SMOOKE, M. 1987*a* Calculation of extinction limits for premixed laminar flames in a stagnation point flow. *J. Comput. Phys.* **68**, 327–345.

GIOVANGIGLI, V. & SMOOKE, M. 1987*b* Extinction of strained premixed laminar flames with complex chemistry. *Combust. Sci. Technol.* **53**, 23–49.

GIOVANGIGLI, V. & SMOOKE, M. 1988 Adaptive continuation algorithms with applications to combustion problems. *Appl. Numer. Math.* **5**, 305.

GIRIMAJI, S. S. & POPE, S. B. 1992 Propagating surfaces in isotropic turbulence. *J. Fluid Mech.* **234**, 247–277.

HAWORTH, D. C. & POINSOT, T. J. 1992 Numerical simulations of Lewis number effects in turbulent premixed flames. *J. Fluid Mech.* **244**, 405–436.

HERRING, J. R., ORSZAG, S. A., KRAICHNAN, R. H. & FOX, D. G. 1974 Decay of two-dimensional homogeneous turbulence. *J. Fluid Mech.* **66**, 417–444.

HINZE, J. O. 1975 *Turbulence*, 2nd edn. McGraw-Hill.

HURLE, I., PRICE, R., SUGDEN, T. & THOMAS, A. 1968 Sound emission from open turbulent premixed flames. *Proc. R. Soc. Lond.* A **303**, 409–427.

JOULIN, G. & MITANI, T. 1981 Linear stability analysis of two-reactant flames. *Combust. Flame* **40**, 235–246.

KEE, R., MILLER, J., EVANS, G. & DIXON-LEWIS, G. 1988 A computational model of the structure and extinction of strained opposed flow, premixed methane air flames. In *22nd Symp. (Intl) on Combustion*, pp. 1479–1494. The Combustion Institute.

KEE, R. J., MILLER, J. A. & JEFFERSON, T. H. 1980 Chemkin: a general-purpose, problem-independent, transportable, fortran chemical-kinetics code package. *Sandia Tech. Rep.* SAND80-8003.

KEE, R. J., WARNATZ, J. & MILLER, J. A. 1983 A fortran computer code package for the evaluation

of gas-phase viscosities, conductivities, and diffusion coefficients. *Sandia Tech. Rep.* SAND83-8209.

KERSTEIN, A. R., ASHURST, W. T. & WILLIAMS, F. A. 1988 Field equations for interface propagation in an unsteady homogeneous flowfield. *Phys. Rev.* A **37**, 2728–2731.

KWON, S., TSENG, L.-K. & FAETH, G. 1992 Laminar burning velocities and transition to unstable flames in $H_2/O_2/N_2$ and $C_3H_8/O_2/N_2$ mixtures. *Combust. Flame* **90**, 230–246.

LEE, T.-W., LEE, J., NYE, D. & SANTAVICCA, D. A. 1993 Local response and surface properties of premixed flames during interactions with kármán vortex streets. *Combust. Flame* **94**, 146–160.

LEE, T.-W., NORTH, G. L. & SANTAVICCA, D. A. 1992 Curvature and orientation statistics of turbulent premixed flame fronts. *Combust. Sci. Technol.* **84**, 121–132.

LELE, S. 1992 Compact finite difference schemes with spectral-like resolution. *J. Comput. Phys.* **103**, 16–42.

LESIEUR, M. 1987 *Turbulence in Fluids*. Martinus Nijhoff.

MANTZARAS, J., FELTON, P. G. & BRACCO, F. V. 1988 Three-dimensional visualization of premixed-charge engine flames. *SAE. Tech. Rep.* 881635.

MENEVEAU, C. & POINSOT, T. 1990 Stretching and quenching of flamelets in premixed turbulent combustion. *Combust. Flame* **86**, 311–332.

MILLER, J. A., MITCHELL, R. E., SMOOKE, M. D. & LEE, R. J. 1982 Toward a comprehensive chemical kinetic mechanism for the oxidation of acetylene: comparison of model predictions with results from flame and shock tube experiments. In *19th Symp. (Intl) on Combustion*, pp. 181–196. The Combustion Institute, Pittsburgh.

MONTGOMERY, C. J., KOSALY, G. & RILEY, J. 1993 Direct numerical simulation of turbulent reacting flow using a reduced hydrogen–oxygen mechanism. *Combust. Flame* **94**, 247–260.

ORAN, E. S. & BORIS, J. P. 1987 *Numerical Simulation of Reactive Flow*, Elsevier.

POINSOT, T. 1991 Flame ignition in a premixed turbulent flow. In *Center for Turbulence Research Annual Research Briefs*, pp. 1–22, Stanford University. Center for Turbulence Research & NASA Ames.

POINSOT, T., ECHEKKI, T. & MUNGAL, M. G. 1992 A study of the laminar flame tip and implications for premixed turbulent combustion. *Combust. Sci. Technol.* **81**, 45–55.

POINSOT, T. J., HAWORTH, D. C. & BRUNEAUX, G. 1993 Direct simulation and modelling of flame-wall interaction for turbulent premixed combustion. *Combust. Flame* **94**, 118–132.

POINSOT, T. & LELE, S. 1992 Boundary conditions for direct simulations of compressible viscous flows. *J. Comput. Phys.* **101**, 104–129.

POINSOT, T., TROUVÉ, A., VEYNANTE, D., CANDEL, S. & ESPOSITO, E. 1987 Vortex driven acoustically coupled combustion instabilities. *J. Fluid Mech.* **177**, 265–292.

POINSOT, T., VEYNANTE, D. & CANDEL, S. 1990 Diagrams of premixed turbulent combustion based on direct simulation. In *23rd Symp. (Intl) on Combustion*, pp. 613–619. The Combustion Institute, Pittsburgh.

POINSOT, T., VEYNANTE, D. & CANDEL, S. 1991 Quenching processes and premixed turbulent combustion diagrams. *J. Fluid Mech.* **228**, 561–606.

POPE, S. B. 1988 Evolution of surfaces in turbulence. *Intl J. Engng. Sci.* **26**, 445–469.

POPE, S. B. 1991 Numerical issues in p.d.f. methods. In *Fourth Intl Conf. on Numerical Combustion*, *St. Petersburg, FL*, p. 165. SIAM.

RUTLAND, C. J., FERZIGER, J. H. & EL TAHRY, S. H. 1990 Full numerical simulation and modeling of turbulent premixed flames. In *23rd Symp. (Intl) on Combustion*, pp. 621–627. The Combustion Institute, Pittsburgh.

RUTLAND, C. & TROUVÉ, A. 1990 Premixed flame simulations for nonunity lewis numbers. In *Proc. 1990 Summer Program*, pp. 299–309, Stanford University. Center for Turbulence Research & NASA Ames.

RUTLAND, C. & TROUVÉ, A. 1993 Direct simulations of premixed turbulent flames with nonunity Lewis numbers. *Combust. Flame* **94**, 41–57.

SEARBY, G. & QUINARD, J. 1990 Direct and indirect measurements of markstein numbers of premixed flames. *Combust. Flame* **82**, 289–311.

SMOOKE, M. 1982 Solution of burner stabilized premixed laminar flames by boundary value method. *J. Comput. Phys.* **48**, 72–105.

SMOOKE, M. D., LIN, P., LAM, J. & LONG, M. B. 1990 Computational and experimental study of a laminar axisymmetric methane–air diffusion flame. In *23rd Symp. (Intl) on Combustion*, pp. 575–582. The Combustion Institute, Pittsburgh.

TROUVÉ, A. & POINSOT, T. 1994 The evolution equation for the flame surface density in turbulent premixed combustion. *J. Fluid Mech.* **278**, 1–31.

WARNATZ, J. 1981 Concentration-, pressure-, and temperature-dependence of the flame velocity in hydrogen–oxygen–nitrogen mixtures. *Combust. Sci. Technol.* **26**, 203–213.

WESTBROOK, C. & DRYER, F. 1984 Chemical kinetic modelling of hydrocarbon combustion. *Prog. Energ. Combust. Sci.* **10**, 1–57.

WU, M., KWON, S., DRISCOLL, J. & FAETH, G. 1990 Turbulent premixed hydrogen/air flames at high reynolds numbers. *Combust. Sci. Technol.* **73**, 327–350.

XU, Y. & SMOOKE, M. D. 1991 Primitive variable solution of a confined laminar diffusion flame using a detailed reaction mechanism. In *Fourth Intl Conf. on Numerical Combustion, St. Petersburg, FL*, pp. 228–229. SIAM.